Journal of the American Statistical Association

ISSN: (Print) (Online) Journal homepage: www.tandfonline.com/journals/uasa20

Bayesian Modeling with Spatial Curvature Processes

Aritra Halder, Sudipto Banerjee & Dipak K. Dey

To cite this article: Aritra Halder, Sudipto Banerjee & Dipak K. Dey (2024) Bayesian Modeling with Spatial Curvature Processes, Journal of the American Statistical Association, 119:546, 1155-1167, DOI: 10.1080/01621459.2023.2177166

To link to this article: https://doi.org/10.1080/01621459.2023.2177166

JOURNAL OF THE AMERICAN STATISTICAL ASSOCIATION
2024, VOL. 119, NO. 546, 1155–1167: Theory and Methods
https://doi.org/10.1080/01621459.2023.2177166

Bayesian Modeling with Spatial Curvature Processes

Aritra Halder[a], Sudipto Banerjee[b], and Dipak K. Dey[c]

[a]Department of Biostatistics, Drexel University, Philadelphia, PA; [b]Department of Biostatistics, University of California, Los Angeles, CA; [c]Department of Statistics, University of Connecticut, Storrs, CT

ABSTRACT

Spatial process models are widely used for modeling point-referenced variables arising from diverse scientific domains. Analyzing the resulting random surface provides deeper insights into the nature of latent dependence within the studied response. We develop Bayesian modeling and inference for rapid changes on the response surface to assess directional curvature along a given trajectory. Such trajectories or curves of rapid change, often referred to as *wombling* boundaries, occur in geographic space in the form of rivers in a flood plain, roads, mountains or plateaus or other topographic features leading to high gradients on the response surface. We demonstrate fully model based Bayesian inference on directional curvature processes to analyze differential behavior in responses along wombling boundaries. We illustrate our methodology with a number of simulated experiments followed by multiple applications featuring the Boston Housing data; Meuse river data; and temperature data from the Northeastern United States. Supplementary materials for this article are available online.

ARTICLE HISTORY
Received May 2022
Accepted January 2023

KEYWORDS
Bayesian modeling;
Directional curvature;
Gaussian processes;
Wombling

1. Introduction

Spatial data science manifests in a variety of domains including environmental and Geographical Information Systems (GIS) (Webster and Oliver 2007; Burrough, McDonnell, and Lloyd 2015; Schabenberger and Gotway 2017; Plant 2018), digital cartography and terrain modeling (Law, Kelton, and Kelton 2000; Santner et al. 2003; Jones 2014; Vaughan 2018), imaging (Winkler 2003; Chiu et al. 2013; Dryden and Mardia 2016), spatial econometrics and land use (LeSage and Pace 2009), public health and epidemiology (Elliot et al. 2000; Waller and Gotway 2004; Lawson 2013) and public policy (Haining 1993; Wise and Craglia 2007). Spatial data analysis seeks to estimate an underlying spatial surface representing the process generating the data. Specific inferential interest resides with local features of the surface including rates of change of the process at points and along "spatial boundaries" to understand the behavior of the underlying process and identify lurking explanatory variables or risk factors. This exercise is often referred to as "wombling", named after a seminal paper by Womble (1951); (also see Gleyze, Bacro, and Allard 2001; Banerjee 2010). For regionally aggregated data, it identifies boundaries delineating neighboring regions and has been used to study health disparities (Lu and Carlin 2005; Li et al. 2015; Gao, Banerjee, and Ritz 2022) and ecological boundaries (Fitzpatrick et al. 2010). For point-referenced data, where variables are mapped at locations within an Euclidean coordinate frame with a sufficiently smooth spatial surface, it refers to estimating spatial gradients and identifying boundaries representing large gradients (Banerjee, Gelfand, and Sirmans 2003; Banerjee and Gelfand 2006; Qu, Bradley, and Niu 2021).

Our current contribution develops Bayesian inference for spatial curvature along curves on Euclidean domains. Modeling curvature will require smoothness considerations of the process (Adler 1981; Kent 1989; Stein 1999; Banerjee and Gelfand 2003). Observations over a finite set of locations from these processes cannot visually inform about smoothness. Therefore, smoothness of the process is specified from mechanistic considerations which can be introduced through prior specifications as needed. While Bayesian inference for first-order derivatives and directional gradients have received considerable attention (see, e.g., Morris, Mitchell, and Ylvisaker 1993; Banerjee, Gelfand, and Sirmans 2003; Majumdar et al. 2006; Liang, Banerjee, and Carlin 2009; Heaton 2014; Terres and Gelfand 2015; Wang and Berger 2016; Terres and Gelfand 2016; Wang, Bhattacharya, and Gelfand 2018; Qu, Bradley, and Niu 2021, for inferential developments involving spatial gradients from diverse modeling and application perspectives) such processes inform about directional change, but do not enable inference on curvature (departure from flatness) of the spatial surface.

Analyzing surface roughness from sampling considerations can be traced at least as far back as Greenwood (1984). We offer full inference with uncertainty quantification about spatial curvature at a point and average curvature along a curve from observed data after accounting for explanatory variables. Considering second-order finite differences we establish a valid spatial curvature process as a limit of such finite difference processes. When formulating directional curvature, we favor the normal direction corresponding to a chosen curve and devise a "wombling" measure to track curvature of the surface

CONTACT Sudipto Banerjee sudipto@ucla.edu Department of Biostatistics, University of California, Los Angeles, CA.
Supplementary materials for this article are available online. Please go to www.tandfonline.com/r/JASA.

along the curve. We derive and exploit analytical expressions of higher order processes to avoid numerical finite differences. The Bayesian inferential framework delivers exact posterior inference for the above constructs on the response as well as latent (or residual) processes.

Section 2 develops the directional curvature processes through a differential operator. Section 3 develops the vector analytic framework for curvilinear wombling using curvature processes. Section 4 builds a hierarchical model to exploit the preceding distribution theory and conduct curvature analysis on the response and the latent process. Section 5 presents detailed simulation experiments for assessing directional gradients and curvatures. Section 6 considers applications to three different datasets: Boston housing data, Meuse river data, and Northeastern U.S. Temperatures (the third data is presented in the supplementary materials).

2. Spatial Curvature Processes

Let $\{Y(\mathbf{s}) : \mathbf{s} \in \mathcal{S} \subset \mathbb{R}^d\}$ be a univariate weakly stationary random field with zero mean, finite second moment and a positive definite covariance function $K(\mathbf{s}, \mathbf{s}') = \text{cov}\left(Y(\mathbf{s}), Y(\mathbf{s}')\right)$ for locations $\mathbf{s}, \mathbf{s}' \in \mathbb{R}^d$. In particular, under *isotropy* we assume $K(\mathbf{s}, \mathbf{s}') = \widetilde{K}\left(||\mathbf{s} - \mathbf{s}'||\right)$, where $||\mathbf{s}-\mathbf{s}'||$ is the Euclidean distance between the locations $\mathbf{s}, \mathbf{s}'$ (Matérn 2013). Building upon notions of mean square smoothness (see, e.g., Stein 1999) at an arbitrary location $\mathbf{s}_0$ in $\mathbb{R}^d$, we focus upon second order differentiability, $Y(\mathbf{s}_0 + h\mathbf{u}) = Y(\mathbf{s}_0) + h\mathbf{u}^\top \nabla Y(\mathbf{s}_0) + h^2\mathbf{u}^\top \nabla^2 Y(\mathbf{s}_0)\mathbf{u}/2 + r_2(\mathbf{s}_0, h^2||\mathbf{u}||)$, where $r_2(\mathbf{s}_0, h^2||\mathbf{u}||)/h^2 \to 0$ as $h \to 0$ in the L_2 sense and ∇ and ∇^2 are the gradient and Hessian operators, respectively.

For the scalar h and unit vectors $\mathbf{u}, \mathbf{v}$, we define $Y^{(2)}_{\mathbf{u},\mathbf{v},h}(\mathbf{s}_0) = (Y(\mathbf{s}_0 + h(\mathbf{u} + \mathbf{v})) - Y(\mathbf{s}_0 + h\mathbf{u}) - Y(\mathbf{s}_0 + h\mathbf{v}) + Y(\mathbf{s}_0))/h^2$ to be the second order finite difference processes in the directions $\mathbf{u}$, $\mathbf{v}$ at scale h. Being a linear function of stationary processes it is well-defined. Passing to limits, $D^{(2)}_{\mathbf{u},\mathbf{v}}Y(\mathbf{s}_0) = \lim_{h\to 0} Y^{(2)}_{\mathbf{u},\mathbf{v},h}(\mathbf{s}_0)$. Provided the limit exists, $D^{(2)}_{\mathbf{u},\mathbf{u}}Y(\mathbf{s}_0)$ is defined as the directional curvature process. If $Y(\mathbf{s})$ is a mean square second order differentiable process in $\mathbb{R}^d$ for every $\mathbf{s} \in \mathbb{R}^d$ then $D^{(2)}_{\mathbf{u},\mathbf{v}}Y(\mathbf{s}) = \mathbf{u}^\top \nabla^2 Y(\mathbf{s})\mathbf{v}$ is well-defined with $D^{(2)}_{\mathbf{u},\mathbf{v}}Y(\mathbf{s}) = \lim_{h\to 0}\left(h^2\mathbf{u}^\top \nabla^2 Y(\mathbf{s})\mathbf{v} + \widetilde{r}_2\right)/h^2 = \mathbf{u}^\top \nabla^2 Y(\mathbf{s})\mathbf{v}$, where $\widetilde{r}_2 = r_2(\mathbf{s}, h^2||\mathbf{u} + \mathbf{v}||) - r_2(\mathbf{s}, h^2||\mathbf{u}||) - r_2(\mathbf{s}, h^2||\mathbf{v}||)$. In practice, we need only work with computing these derivatives for an orthonormal basis of $\mathbb{R}^d$, say the Euclidean canonical unit vectors along each axis $\{\mathbf{e}_1, \ldots, \mathbf{e}_d\}$. If $\mathbf{u} = \sum_{i=1}^d u_i\mathbf{e}_i$, and $\mathbf{v} = \sum_{i=1}^d v_i\mathbf{e}_i$ are arbitrary unit vectors, we can compute $D^{(2)}_{\mathbf{u},\mathbf{v}}Y(\mathbf{s}) = \sum_{i=1}^d \sum_{j=1}^d u_i D^{(2)}_{\mathbf{e}_i,\mathbf{e}_j}Y(\mathbf{s})v_j$. The directional curvature process is linear in the sense that $D^{(2)}_{-\mathbf{u},-\mathbf{v}}Y(\mathbf{s}) = D^{(2)}_{\mathbf{u},\mathbf{v}}Y(\mathbf{s})$, $D^{(2)}_{\mathbf{u},-\mathbf{v}}Y(\mathbf{s}) = D^{(2)}_{-\mathbf{u},\mathbf{v}}Y(\mathbf{s}) = -D^{(2)}_{\mathbf{u},\mathbf{v}}Y(\mathbf{s})$. Since $D^{(2)}_{\mathbf{w},\mathbf{w}}Y(\mathbf{s}) = ||\mathbf{w}||^2 D^{(2)}_{\mathbf{u},\mathbf{u}}Y(\mathbf{s})$, where $\mathbf{w} = ||\mathbf{w}||\mathbf{u}$ and $\mathbf{u}$ is a unit direction, we henceforth only consider unit directions. First-order directional gradient processes, $D^{(1)}_{\mathbf{u}}Y(\mathbf{s})$, are reviewed in Banerjee and Gelfand (2006) and in Section S1.1 of the supplementary materials. Choosing a direction is emphasized with respect to interpreting the directional curvature processes. Directional curvature is the change in the normal to the surface $Y(\mathbf{s})$ at $\mathbf{s}_0$ when moving along a slice of the surface in the direction $\mathbf{w}$. The associated algebraic sign locally classifies the nature of curvature at $\mathbf{s}_0$—for instance, convex or concave ellipsoids (see Stevens 1981). A detailed discussion, with illustration, is available in Section S2 of the supplementary materials.

Since $\nabla^2 Y(\mathbf{s})$ is a symmetric matrix, to avoid singularities arising from duplication we modify $D^{(2)}_{\mathbf{u},\mathbf{v}}Y(\mathbf{s})$ as follows. If vech is the usual half-vectorization operator for symmetric matrices and $\mathcal{D}_d$ is the duplication matrix (Magnus and Neudecker 1980) of order $d^2 \times d(d+1)/2$ then, $D^{(2)}_{\mathbf{u},\mathbf{v}}Y(\mathbf{s}) = \mathbf{c}^\top_{\mathbf{u},\mathbf{v}}\text{vech}\left(\nabla^2 Y(\mathbf{s})\right)$ where $\mathbf{c}^\top_{\mathbf{u},\mathbf{v}} = (\mathbf{u} \otimes \mathbf{v})^\top \mathcal{D}_d$ and $\otimes$ is the Kronecker product for matrices. If $\mathbf{u} = (u_1, u_2)^\top, \mathbf{v} = (v_1, v_2)^\top \in \mathbb{R}^2$, then $\mathbf{c}_{\mathbf{u},\mathbf{v}} = (\mathbf{u} \otimes \mathbf{v})^\top \mathcal{D}_2 = (v_1u_1, v_1u_2 + v_2u_1, v_2u_2)^\top$. The process $\text{vech}\left(\nabla^2 Y(\mathbf{s})\right)$ in $\mathbb{R}^{d(d+1)/2}$ consists of the pure and mixed second order derivatives in $\nabla^2 Y(\mathbf{s})$. The distributions needed for inference on directional curvature processes depend on $\text{vech}\left(\nabla^2 Y(\mathbf{s})\right)$ rather than $\nabla^2 Y(\mathbf{s})$. We refer to $(\nabla Y(\mathbf{s})^\top, \text{vech}(\nabla^2 Y(\mathbf{s}))^\top)^\top$ as the differential process and $\{\mathbf{u}^\top \nabla Y(\mathbf{s}), \mathbf{c}^\top_{\mathbf{u},\mathbf{u}}\text{vech}(\nabla^2 Y(\mathbf{s}))\}$ as the directional differential processes induced by $Y(\mathbf{s})$ along $\mathbf{u}$.

Inference for differential processes requires $(Y(\mathbf{s}), \nabla Y(\mathbf{s})^\top, \text{vech}(\nabla^2 Y(\mathbf{s}))^\top)$ to be a valid multivariate process. Its existence is derived from the limit of corresponding finite difference approximations, which yields the cross-covariance matrix depending on fourth (and lower) order derivatives of K. We investigate the parent and differential processes using a differential operator $\mathcal{L} : \mathbb{R}^1 \to \mathbb{R}^m$, $m = 1+d+d(d+1)/2$, where $\mathcal{L}Y = \left(Y, \nabla Y^\top, \text{vech}(\nabla^2 Y)^\top\right)^\top$. The resulting process $\mathcal{L}Y(\mathbf{s})$ is also stationary with a zero mean and a cross-covariance matrix

$$V_{\mathcal{L}Y}(\Delta) = \begin{pmatrix} K(\Delta) & -(\nabla K(\Delta))^\top & \text{vech}(\nabla^2 K(\Delta))^\top \\ \nabla K(\Delta) & -\nabla^2 K(\Delta) & \nabla^3 K(\Delta)^\top \\ \text{vech}(\nabla^2 K(\Delta)) & -\nabla^3 K(\Delta) & \nabla^4 K(\Delta) \end{pmatrix}, \tag{1}$$

where $\Delta = \mathbf{s} - \mathbf{s}'$, $\nabla K(\Delta)$ is the $d \times 1$ gradient, $\nabla^2 K(\Delta)$ is the $d \times d$ Hessian, $\nabla^3 K(\Delta)$ is the $d(d+1)/2 \times d$ matrix of third derivatives and $\nabla^4 K(\Delta)$ is the $d(d+1)/2 \times d(d+1)/2$ matrix of fourth order derivatives associated with $K(\Delta)$. Under isotropy, $\nabla K(\Delta) = \frac{\nabla \widetilde{K}(||\Delta||)}{||\Delta||}\Delta$, if $A_0 = \left(\nabla^2 \widetilde{K}(||\Delta||) - \frac{\nabla \widetilde{K}(||\Delta||)}{||\Delta||}\right)$ then, $\nabla^2 K(\Delta) = \frac{\nabla \widetilde{K}(||\Delta||)}{||\Delta||} I_d + A_0 \frac{\Delta\Delta^\top}{||\Delta||^2}$, $\nabla^3 K(\Delta) = A_0\left\{\frac{\text{vech}(I_d)^\top \otimes \Delta}{||\Delta||^2} - 3\frac{\text{vech}(\Delta\Delta^\top)^\top \otimes \Delta}{||\Delta||^4} + \frac{1}{||\Delta||^2}\left(\frac{\partial \text{vech}(\Delta\Delta^\top)}{\partial \Delta}\right)\right\} + \nabla^3 \widetilde{K}(||\Delta||) \cdot \frac{\text{vech}(\Delta\Delta^\top)^\top \otimes \Delta}{||\Delta||^3}$, where $\widetilde{K}(\Delta)$ and its derivatives are analytically computed for our covariance functions of interest in Section S3 of the supplementary materials. Let $A_1 = \frac{\partial \Delta \otimes \text{vech}(I_d)^\top}{\partial \Delta}$, $A_2 = \frac{\partial \Delta \otimes \text{vech}(\Delta\Delta^\top)^\top}{\partial \Delta}$, $A_3 = \frac{\partial}{\partial \Delta}\left(\frac{\partial \text{vech}(\Delta\Delta^\top)}{\partial \Delta}\right)$ be reordered tensors (matrices) of order $d(d+1)/2 \times d(d+1)/2$ conforming to the order of corresponding elements in vech. Let A_4 be the element-wise product of Δ with $\left(\frac{\partial \text{vech}(\Delta\Delta^\top)}{\partial \Delta}\right)$ in the same order, $B_1 = \text{vech}(\Delta\Delta^\top)\text{vech}(I_d)^\top$ and $B_2 = \text{vech}(\Delta\Delta^\top)\text{vech}(\Delta\Delta^\top)^\top$. Then, $\nabla^4 K(\Delta)$ is,

$$A_0\left\{\frac{A_1}{||\Delta||^2}-3\frac{A_2}{||\Delta||^4}+\frac{A_3}{||\Delta||^2}-(1+A_4)\left(\frac{2B_1}{||\Delta||^4}+\frac{B_1}{||\Delta||^3}\right)+3\left(\frac{4B_2}{||\Delta||^6}+\frac{B_2}{||\Delta||^5}\right)\right\}+\nabla^3\widetilde{K}(||\Delta||)\left(\frac{B_1}{||\Delta||^3}+\frac{A_2}{||\Delta||^3}+\frac{A_4}{||\Delta||^3}-6\frac{B_2}{||\Delta||^5}\right)+\nabla^4\widetilde{K}(||\Delta||)\frac{B_2}{||\Delta||^4}\,. \tag{2}$$

The resulting multivariate differential process, $\mathcal{L}Y$, is stationary but not isotropic. Evidently, for the differential operator to be well-defined under isotropy, $\nabla^4 K(\mathbf{0})$ must exist since $\text{var}(D^{(2)}_{\mathbf{u},\mathbf{u}}Y(\mathbf{s})) = \nabla^4\widetilde{K}(\mathbf{0})$ (analogous to results in Banerjee, Gelfand, and Sirmans 2003, sec. 3). The directional differential operator is defined analogously as $\mathcal{L}_{\mathbf{u}}Y(\mathbf{s})$ such that $\mathcal{L}_{\mathbf{u}} : \mathbb{R} \to \mathbb{R}^3$. If $a_0 = \left(1-\frac{(\mathbf{u}^\top\Delta)^2}{||\Delta||^2}\right)$, then analogous to (2) the covariance function of the directional curvature process, $\text{cov}\left(\mathbf{c}^\top_{\mathbf{u},\mathbf{u}}\text{vech}(\nabla^2 Y(\mathbf{s})), \mathbf{c}^\top_{\mathbf{u},\mathbf{u}}\text{vech}(\nabla^2 Y(\mathbf{s}'))\right) = \frac{3}{||\Delta||^2}(5a_0-4)a_0A_0 + \frac{6}{||\Delta||}(1-a_0)a_0\nabla^3\widetilde{K}(||\Delta||) + (1-a_0)^2\nabla^4\widetilde{K}(||\Delta||)$. To characterize covariance functions that admit such processes, we turn to spectral theory. Recall that for a positive definite function K defined in $\mathbb{R}$, Bochner's theorem (see, e.g., Williams and Rasmussen 2006) establishes the existence of a finite positive spectral measure $\mathcal{F}$ on $\mathbb{R}$. K can be expressed as the inverse Fourier transform of $\mathcal{F}$, $K(t) = \int_{\mathbb{R}} e^{-i\lambda t}\mathcal{F}(d\lambda)$. In cases where $\mathcal{F}$ admits a spectral density, $K(t) = \int e^{-i\lambda t}f(\lambda)\,d\lambda$. For $\nabla^4 K$ to exist, a trivial extension of the result in Wang, Bhattacharya, and Gelfand (2018) requires that f possess a finite fourth moment. Examples of covariance kernels that satisfy this condition are (a) the squared exponential covariance kernel with $K(t) = \exp(-t^2)$ ($\sigma^2 = \phi = 1$), and $f(\lambda) = 1/2\sqrt{\pi}\exp(-\lambda^2/4)$ then, $\frac{1}{2\sqrt{\pi}}\int_{\mathbb{R}}\lambda^4\exp(-\lambda^2/4)\,d\lambda = 3(\sqrt{2})^4 = 12$; and (b) the Matérn class with fractal parameter, ν; $f(\lambda)$ is known to belong to the t-family (see, e.g., Stein 1999) with $f(\lambda) = C(\phi,\nu)/(c(\phi,\nu)+\lambda^2)^{\nu+1/2}$ then, $\int_{\mathbb{R}}\lambda^4 C(\phi,\nu)/(c(\phi,\nu)+\lambda^2)^{\nu+1/2}\,d\lambda < \infty$, for all $\nu > 2$ (since the fourth central moment for the t-distribution exists if $\nu > 2$). Here, we consider formulating the directional differential processes using these two classes of covariance functions (a) the squared exponential, $\widetilde{K}(||\Delta||) = \sigma^2\exp(-\phi||\Delta||^\nu)$, $\nu = 2$; and (b) members of the Matérn class, $\widetilde{K}(||\Delta||) = \sigma^2(\phi||\Delta||)^\nu K_\nu(\phi||\Delta||)$, where K_ν is the modified Bessel function of order ν (see, e.g., Abramowitz, Stegun, and Romer 1988), and ν controls the smoothness of process realizations. We are particularly interested in $\nu = 5/2$.

The multivariate process, $\mathcal{L}Y(\mathbf{s})$, is valid under the above assumptions without any further specific parametric assumptions over what has been outlined above. To facilitate inference for $\mathcal{L}Y(\mathbf{s})$, a probability distribution is specified for the parent process. We assume that $Y(\mathbf{s}) \sim \text{GP}(\mu(\mathbf{s},\boldsymbol{\beta}), K(\cdot;\sigma^2,\phi))$ is a stationary process specified on $\mathbb{R}^d$. In what follows we also assume that $K = K(\cdot;\sigma^2,\phi)$ admits four derivatives. There are some immediate implications of a Gaussian assumption on the parent process. If $Y_1(\cdot)$ and $Y_2(\cdot)$ are zero mean, independent stationary Gaussian processes on $\mathbb{R}^d$, then (i) the differential processes $\mathcal{L}Y_1$ and $\mathcal{L}Y_2$ are independent of each other; (ii) if $c_1, c_2 \in \mathbb{R}$ are scalars, then $\mathcal{L}(c_1Y_1 + c_2Y_2) = c_1\mathcal{L}Y_1 + c_2\mathcal{L}Y_2$ is stationary and (iii) any sub-vector of $\mathcal{L}Y$, for example Y or $(Y, \nabla Y^\top)^\top$, is a stationary Gaussian processes.

If K is k-times mean square differentiable (i.e., $\nabla^{2k}K$ exists), the proposed differential operator can be extended to include higher order derivatives of $\nabla^k Y(\mathbf{s})$ (Mardia et al. 1996). Differential operators characterizing change in the response (and gradient) surface also follow valid stationary Gaussian processes. For instance, at an arbitrary location $\mathbf{s}_0$ the divergence operator, $\text{div}(Y(\mathbf{s}_0)) = \sum_{i=1}^{d}\frac{\partial}{\partial\mathbf{e}_i}Y(\mathbf{s}_0) = \mathbf{c}_1^\top\mathcal{L}Y(\mathbf{s}_0)$, where $\mathbf{c}_1$ is an $m \times 1$ vector with 0's in all places except for first-order derivatives where it takes a value of 1, and the Laplacian, defined as the divergence operator for gradients, $\Delta(Y(\mathbf{s}_0)) = \sum_{i=1}^{d}(\nabla^2 Y(\mathbf{s}_0))_{ii} = \sum_{i=1}^{d}\frac{\partial^2}{\partial\mathbf{e}_i^2}Y(\mathbf{s}_0) = \mathbf{c}_2^\top\mathcal{L}Y(\mathbf{s}_0)$, where $\mathbf{c}_2$ is a $m \times 1$ vector with 0's in all places except for pure second order derivatives where it takes a value of 1. Furthermore, they follow valid Gaussian processes with $\text{var}(\text{div}(Y(\mathbf{s}_0))) = \mathbf{c}_1^\top V_{\mathcal{L}}\mathbf{c}_1$ and $\text{var}(\Delta(Y(\mathbf{s}_0))) = \mathbf{c}_2^\top V_{\mathcal{L}}\mathbf{c}_2$.

Let $Y(\mathbf{s})$ be a Gaussian parent process with a twice-differentiable mean function $\mu(\mathbf{s},\boldsymbol{\beta})$, that is, $\nabla\mu(\mathbf{s},\boldsymbol{\beta})$ and $\nabla^2\mu(\mathbf{s},\boldsymbol{\beta})$ exist, and let $K(\cdot)$ be a covariance function with variance σ^2 and range ϕ. Let $\mathbf{Y} = (Y(\mathbf{s}_1),\ldots,Y(\mathbf{s}_L))^\top$ be the observed realization over $\mathcal{S}$ with mean $\boldsymbol{\mu} = (\mu(\mathbf{s}_1,\boldsymbol{\beta}),\ldots,\mu(\mathbf{s}_L,\boldsymbol{\beta}))^\top$ and $\Sigma_{\mathbf{Y}}$ be the associated $L \times L$ covariance matrix with elements $K(\mathbf{s}_i,\mathbf{s}_j)$, and $\mathbf{s}_0$ be an arbitrary location. Let $\nabla\mathbf{K}_1 = \left(\nabla K(\delta_1)^\top,\ldots,\nabla K(\delta_L)^\top\right)^\top$ and $\nabla\mathbf{K}_2 = \left(\text{vech}(\nabla^2 K(\delta_1))^\top,\ldots,\text{vech}(\nabla^2 K(\delta_L))^\top\right)^\top$ be $L\times d$ and $L\times d(d+1)/2$ matrices, respectively, and $\delta_i = \mathbf{s}_i - \mathbf{s}_0$, $i = 1,\ldots,L$. The distribution $P(\mathbf{Y}, \nabla Y(\mathbf{s}_0), \text{vech}(\nabla^2 Y(\mathbf{s}_0)) \mid \boldsymbol{\theta})$, where $\boldsymbol{\theta} = \{\boldsymbol{\beta},\sigma^2,\phi\}$, is the $m_0 = L + d + d(d+1)/2$-dimensional Gaussian,

$$\mathcal{N}_{m_0}\left(\begin{pmatrix}\boldsymbol{\mu}\\ \nabla\mu(\mathbf{s}_0)\\ \text{vech}(\nabla^2\mu(\mathbf{s}_0))\end{pmatrix}, \begin{pmatrix}\Sigma_{\mathbf{Y}} & -\nabla\mathbf{K}_1 & \nabla\mathbf{K}_2\\ \nabla\mathbf{K}_1^\top & -\nabla^2 K(\mathbf{0}) & \nabla^3 K(\mathbf{0})\\ \nabla\mathbf{K}_2^\top & -\nabla^3 K(\mathbf{0})^\top & \nabla^4 K(\mathbf{0})\end{pmatrix}\right), \tag{3}$$

which is well-defined as long as the fourth order derivative of K exists. The posterior predictive distribution for the differential process at $\mathbf{s}_0$ is

$$P(\nabla Y(\mathbf{s}_0), \text{vech}(\nabla^2 Y(\mathbf{s}_0)) \mid \mathbf{Y}) = \int P(\nabla Y(\mathbf{s}_0), \text{vech}(\nabla^2 Y(\mathbf{s}_0)) \mid \mathbf{Y},\boldsymbol{\theta})P(\boldsymbol{\theta} \mid \mathbf{Y})\,d\boldsymbol{\theta}\,. \tag{4}$$

Posterior inference for curvature proceeds by sampling from $P(\text{vech}(\nabla^2 Y(\mathbf{s}_0)) \mid \mathbf{Y}) = \int P(\text{vech}(\nabla^2 Y(\mathbf{s}_0)) \mid \nabla Y(\mathbf{s}_0),\mathbf{Y},\boldsymbol{\theta})P(\nabla Y(\mathbf{s}_0) \mid \mathbf{Y},\boldsymbol{\theta})P(\boldsymbol{\theta} \mid \mathbf{Y})\,d\boldsymbol{\theta}\,d\nabla Y$. We sample from (4) by drawing one instance of $(\nabla Y(\mathbf{s}_0), \text{vech}(\nabla^2 Y(\mathbf{s}_0)))$ for each sample of $\boldsymbol{\theta}$ obtained from $P(\boldsymbol{\theta} \mid \mathbf{Y})$. The conditional predictive distribution of the differential process is given by $\nabla Y(\mathbf{s}_0), \text{vech}(\nabla^2 Y(\mathbf{s}_0)) \mid \mathbf{Y},\boldsymbol{\theta} \sim \mathcal{N}_{m_1}(\boldsymbol{\mu}_1,\Sigma_1)$ where $m_1 = d + d(d+1)/2$, and

$$\boldsymbol{\mu}_1 = \begin{pmatrix}\nabla\mu(\mathbf{s}_0)\\ \text{vech}(\nabla^2\mu(\mathbf{s}_0))\end{pmatrix} - \begin{pmatrix}\nabla\mathbf{K}_1\\ \nabla\mathbf{K}_2\end{pmatrix}^\top\Sigma_{\mathbf{Y}}^{-1}(\mathbf{Y}-\boldsymbol{\mu})\,, \tag{5}$$

$$\Sigma_1 = \begin{pmatrix} -\nabla^2 K(\mathbf{0}) & \nabla^3 K(\mathbf{0})^\top \\ -\nabla^3 K(\mathbf{0}) & \nabla^4 K(\mathbf{0}) \end{pmatrix} - \begin{pmatrix} \nabla \mathbf{K}_1 \\ \nabla \mathbf{K}_2 \end{pmatrix}^\top \Sigma_{\mathbf{Y}}^{-1} \begin{pmatrix} -\nabla \mathbf{K}_1 \\ \nabla \mathbf{K}_2 \end{pmatrix}. \tag{6}$$

Analogous results follow for posterior predictive inference on the curvature process.

If $\mu(\mathbf{s}, \boldsymbol{\beta}) = \mu$ is a constant, as in simple "kriging," then $\nabla\mu(\mathbf{s}) = \nabla^2\mu(\mathbf{s}) = 0$. More generally, if $\mu(\mathbf{s}, \boldsymbol{\beta}) = \mathbf{x}(\mathbf{s})^\top\boldsymbol{\beta}$, where $\mathbf{x}(\mathbf{s})$ is a vector of spatially indexed covariates and $\mathbf{x}(\mathbf{s})^\top\boldsymbol{\beta}$ produces a twice differentiable trend surface then explicit calculation of $\nabla\mu(\mathbf{s}_0)$ and $\nabla^2\mu(\mathbf{s}_0)$ are possible. In case $Y(\mathbf{s}) = \mu(\mathbf{s}, \boldsymbol{\beta}) + Z(\mathbf{s}) + \epsilon(\mathbf{s})$, where $Z(\mathbf{s}) \sim \text{GP}(\mathbf{0}, K(\cdot; \sigma^2, \phi))$ and $\epsilon(\mathbf{s}) \sim N(0, \tau^2)$ is a white-noise process, inference on gradients for the residual spatial process, $Z(\mathbf{s})$, can be performed from the posterior predictive distribution, $P(\nabla Z(\mathbf{s}_0), \text{vech}(\nabla^2 Z(\mathbf{s}_0)) \mid \mathbf{Y})$. We address this in Section 4 in the context of curvature wombling.

3. Wombling with Curvature Processes

Bayesian wombling deals with inference for line integrals

$$\Gamma(C) = \int_C g(\mathcal{L}Y)\, \mathrm{d}\ell \quad \text{or,} \quad \overline{\Gamma}(C) = \frac{1}{\ell(C)} \int_C g(\mathcal{L}Y)\, \mathrm{d}\ell\,, \tag{7}$$

where C is a geometric structure of interest, such as lines or planar curves, residing within the spatial domain of reference, ℓ is an appropriate measure, often taken to be the arc-length measure, g is a linear function (or functional) of the differential operator $\mathcal{L}Y$. Γ and $\overline{\Gamma}$ are referred to as the total and average *wombling measures*, respectively. The structure C is defined to be a *wombling boundary* if it yields a large total (or average) wombling measure. Depending on the spatial domain, geometric structures of interest constructed within them may vary. For example, if we are dealing with surfaces in $\mathbb{R}^3$, choices of C are curves and lines within the surface, with the local co-ordinate being $\mathbb{R}^2$. In higher dimensions they would be planes (curves) or hyperplanes (hypercurves). Specifically, Bayesian curvilinear wombling involves estimating integrals in (7) over curves, which tracks rapid change over the spatial domain by determining boundaries (curves) with large gradients normal to the curve (see for e.g., Banerjee and Gelfand 2006). The integrand in (7) inherently involves a direction, in particular change measured is always in a direction normal to C. Hence, $g(\mathcal{L}Y)$ can equivalently be expressed as a linear function (functional) of $\mathcal{L}_{\mathbf{n}}Y(\mathbf{s})$, where $\mathbf{n} = \mathbf{n}(\mathbf{s})$ denotes the unit normal vector to C at $\mathbf{s}$. The next few paragraphs provide more detail.

With wombling measures for directional gradients discussed the Section S1.2, supplementary materials, we construct wombling measures for curvature. Given C, depending on the smoothness of the surface, the rate at which gradients change along the curve may present sufficient heterogeneity while traversing the curve. If C forms a wombling boundary with respect to the gradient, then wombling boundaries for curvature are subsets of C that feature segments with large positive (negative) directional curvature along a normal direction to the curve. Leveraging only gradients, we develop wombling measures for curvature that further characterize such boundaries located for gradients. The wombling measure for curvature in $Y(\mathbf{s})$ along C ascertains whether C also forms a wombling boundary with respect to curvature. We associate a directional curvature to each $\mathbf{s} \in C$, $g(\mathcal{L}Y(\mathbf{s})) = D^{(2)}_{\mathbf{n},\mathbf{n}}Y(\mathbf{s}) = \mathbf{c}^\top_{\mathbf{n},\mathbf{n}}\text{vech}(\nabla^2 Y(\mathbf{s}))$ (a linear function of $\mathcal{L}_{\mathbf{n}}Y(\mathbf{s})$) along the direction of a unit normal $\mathbf{n} = \mathbf{n}(\mathbf{s})$ to C at $\mathbf{s}$. Using (7) we define *wombling measures* for total and average curvature as,

$$\Gamma^{(2)}(C) = \int_C D^{(2)}_{\mathbf{n},\mathbf{n}}Y(\mathbf{s})d\ell = \int_C \mathbf{n}(\mathbf{s})^\top\nabla^2 Y(\mathbf{s})\mathbf{n}(\mathbf{s})d\ell\,,$$
$$\overline{\Gamma}^{(2)}(C) = \Gamma^{(2)}(C)/\ell(C)\,, \tag{8}$$

respectively, where $\ell(C)$ denotes the arc-length of C. Parameterized curves, $C = \{\mathbf{s}(t) = (s_1(t), s_2(t)) : t \in \mathcal{T} \subset \mathbb{R}\}$, offer further insights. As t varies over its domain, $\mathbf{s}(t)$ outlines the curve C. Implicitly assuming that C is regular, that is, $||\mathbf{s}'(t)|| \neq 0$, allows the tangent and normal to exist at all points on the curve. The unit tangent and normal at each point of the curve are $\mathbf{s}'(t)/||\mathbf{s}'(t)||$ and $\mathbf{n} = \mathbf{n}(\mathbf{s}(t)) = (s_2'(t), -s_1'(t))^\top/||\mathbf{s}'(t)||$, respectively, while $\mathbf{c}_{\mathbf{n},\mathbf{n}} = \mathbf{c}_{\mathbf{n}(\mathbf{s}(t)),\mathbf{n}(\mathbf{s}(t))} = (\mathbf{n}(\mathbf{s}(t)) \otimes \mathbf{n}(\mathbf{s}(t)))^\top \mathcal{D}_d$ from Section 2.

The arc-length of C is $\ell(C) = \int_{\mathcal{T}} ||\mathbf{s}'(t)||\, dt$ or $\mathrm{d}\ell = ||\mathbf{s}'(t)||\, dt$. If $\mathcal{T} = [t_0, t_1]$, then $\ell(C) = \int_{t_0}^{t_1} ||\mathbf{s}'(t)||\, dt$ and $\Gamma^{(2)}(C) = \int_{t_0}^{t_1} \mathbf{n}(\mathbf{s}(t))^\top\nabla^2 Y(\mathbf{s}(t))\mathbf{n}(\mathbf{s}(t))||\mathbf{s}'(t)||\, dt$. If C is an open curve, then $\ell(C)^{-1}\int_C \mathbf{n}(\mathbf{s})^\top\nabla^2 Y(\mathbf{s})\mathbf{n}(\mathbf{s})d\mathbf{s} = \ell(C)^{-1}$ $\int_C \mathbf{n}(\mathbf{s}(t))^\top\nabla^2 Y(\mathbf{s}(t))\mathbf{n}(\mathbf{s}(t))||\mathbf{s}'(t)||\, dt$ is the average directional curvature. For example, $C = \{\mathbf{s}(t) = (r\cos t, r\sin t), t \in [0, \pi/4]\}$ is the arc of a parameterized circle of radius r. It follows that $||\mathbf{s}'(t)|| = r$, $\mathbf{n}(\mathbf{s}(t)) = (\cos t, \sin t)^\top$ and $\ell(C)^{-1}$ $\int_0^{\pi/4} \mathbf{n}(\mathbf{s}(t))^\top\nabla^2 Y(\mathbf{s}(t))\mathbf{n}(\mathbf{s}(t))r\, dt = \frac{4}{\pi}\int_0^{\pi/4} \mathbf{n}(\mathbf{s}(t))^\top\nabla^2 Y(\mathbf{s}(t))$ $\mathbf{n}(\mathbf{s}(t))\, dt$. The average curvature in the tangential direction of C is $\frac{1}{\ell(C)}\int_C \mathbf{u}(\mathbf{s}(t))^\top\nabla^2 Y(\mathbf{s}(t))\mathbf{u}(\mathbf{s}(t))||\mathbf{s}'(t)||\, dt = \ell(C)^{-1}$ $\int_{t_0}^{t_1} \frac{\mathbf{s}'(t)}{||\mathbf{s}'(t)||}^\top\nabla^2 Y(\mathbf{s}(t))\frac{\mathbf{s}'(t)}{||\mathbf{s}'(t)||}||\mathbf{s}'(t)||\, dt = \mathbf{u}(\mathbf{s}(t_1))^\top\nabla Y(\mathbf{s}(t_1)) -$ $\mathbf{u}(\mathbf{s}(t_0))^\top\nabla Y(\mathbf{s}(t_0))$. Hence, the average directional curvature remains path independent and is the difference of directional gradient at the endpoints of C.

For a closed curve C, $\oint_C \mathbf{n}(\mathbf{s})^\top\nabla^2 Y(\mathbf{s})\mathbf{n}(\mathbf{s})d\mathbf{s} = \oint_C \mathbf{n}(\mathbf{s}(t))^\top\nabla^2 Y(\mathbf{s}(t))\mathbf{n}(\mathbf{s}(t))||\mathbf{s}'(t)||\, dt$. If the surface admits up to three derivatives, that is, $\nabla^3 Y(\mathbf{s})$ exists, the average curvature of the region, $\mathcal{D}$, enclosed by C, is free of t. If $\mathbf{F}(\mathbf{s}) = \nabla^2 Y(\mathbf{s}) = (F_{ij}(\mathbf{s}))_{i,j=1,2}$, with $F_{12}(\mathbf{s}) = F_{21}(\mathbf{s})$ and $F_{ij} = F_{ij}(\mathbf{s}) = \frac{\partial^2}{\partial s_i \partial s_j}Y(\mathbf{s})$ then, $\oint_C \mathbf{n}(\mathbf{s})^\top\nabla^2 Y(\mathbf{s})\mathbf{n}(\mathbf{s})d\mathbf{s} = \oint_C \mathbf{n}(\mathbf{s})^\top\mathbf{F}(\mathbf{s})\mathbf{n}(\mathbf{s})d\mathbf{s} = \oint_C \mathbf{n}(\mathbf{s}(t))^\top\mathbf{F}(\mathbf{s})\mathbf{n}(\mathbf{s}(t))||\mathbf{s}'(t)||\, dt = \oint_C ||\mathbf{s}'(t)||^{-1}\left(F_{11}s_2'(t)^2 - 2F_{12}s_1'(t)s_2'(t) + F_{22}s_1'(t)^2\right) dt =$ $\iint_{\mathcal{D}} \left\{\frac{\partial F_{11}n_2}{\partial s_1} + \left(\frac{\partial F_{12}n_2}{\partial s_2} + \frac{\partial F_{12}n_1}{\partial s_1}\right) + \frac{\partial F_{22}n_1}{\partial s_2}\right\} ds_1 ds_2$. The last equality is obtained using Green's theorem (see, e.g., Rudin 1976). This can be interpreted as "flux" in the gradient within $\mathcal{D}$. Since, $F_{ij}(\mathbf{s}) = \nabla^2_{ij}Y(\mathbf{s})$, the integrand in the last equality require the existence of $\nabla^3_{ijk}Y(\mathbf{s})$, $i, j, k = 1, 2$. Denoting, $\widetilde{\nabla}^3 Y(\mathbf{s}) = (\nabla^3_{ijk}Y(\mathbf{s}))^\top_{i,j,k=1,2}$, vector of unique third derivatives, and $\mathbf{n}_0(\mathbf{s}) = (n_2(\mathbf{s}), n_2(\mathbf{s}), n_1(\mathbf{s}), n_1(\mathbf{s}))^\top$ then,

$$\frac{1}{\ell(C)}\oint_C \mathbf{c}^\top_{\mathbf{n},\mathbf{n}}\text{vech}(\nabla^2 Y(\mathbf{s}))\, d\mathbf{s} = \frac{1}{\ell(C)}\iint_{\mathcal{D}} \mathbf{n}_0(\mathbf{s})^\top\widetilde{\nabla}^3 Y(\mathbf{s})\, d\mathbf{s}. \tag{9}$$

This extends the development in Section 3.2 of Banerjee and Gelfand (2006) to study the behavior of spatial curvature over closed curves on surfaces in $\mathbb{R}^3$. Sampling along C is generally harder than sampling inside $\mathcal{D}$. Hence, the computational implications of (9) are more appealing. When studying the same behavior along a tangential direction to C with $\mathbf{s}(t_0) = \mathbf{s}(t_1) = \mathbf{s}_0$, $\oint_C \mathbf{u}(\mathbf{s})^\top \nabla^2 Y(\mathbf{s})\mathbf{u}(\mathbf{s})d\mathbf{s} = \oint_{\mathbf{s}(t_0)}^{\mathbf{s}(t_1)} F_{11}(\mathbf{s})n_1 ds_1 + F_{12}(\mathbf{s})n_1 ds_2 + F_{21}(\mathbf{s})n_2 ds_1 + F_{22}(\mathbf{s})n_2 ds_2 = \mathbf{u}(\mathbf{s}(t_1))^\top \nabla Y(\mathbf{s}(t_1)) - \mathbf{u}(\mathbf{s}(t_0))^\top \nabla Y(\mathbf{s}(t_0)) = 0$, again a consequence of path independence. This validates the choice of a normal direction to C when measuring change in the gradient. Using the rectilinear approximation to curvature wombling, as discussed later, provides a more computationally tractable and simpler approach, where double integrals manifest when computing variances of the wombling measures.

Curvature wombling requires predictive inference performed using gradient measures on the interval $\mathcal{T}$, to include $\Gamma^{(2)}(C)$ (or $\overline{\Gamma}^{(2)}(C)$) in (8). Leveraging inference for differential processes in Section 2, we obtain joint inference on the wombling measures. Suppose $C = \{\mathbf{s}(t) : t \in [0,T]\}$ is generated over $\mathcal{T} = [0,T]$. For any $t^* \in [0,T]$, let C_{t^*} denote the curve restricted to $[0,t^*]$ and $\ell(C_{t^*})$ its arc-length. Line integrals for curvilinear gradient and curvature wombling measures are $\Gamma^{(1)}(C_{t^*}) = \int_0^{t^*} D^{(1)}_{\mathbf{n}} Y(\mathbf{s}(t))||\mathbf{s}'(t)||\,dt$, $\overline{\Gamma}^{(1)}(C_{t^*}) = \frac{1}{\ell(C_{t^*})}\Gamma^{(1)}(C_{t^*})$, $\Gamma^{(2)}(C_{t^*}) = \int_0^{t^*} D^{(2)}_{\mathbf{n},\mathbf{n}} Y(\mathbf{s}(t))||\mathbf{s}'(t)||\,dt$ and $\overline{\Gamma}^{(2)}(C_{t^*}) = \frac{1}{\ell(C_{t^*})}\Gamma^{(2)}(C_{t^*})$. Since $D^{(1)}_{\mathbf{n}} Y(\mathbf{s}(t))$ and $D^{(2)}_{\mathbf{n},\mathbf{n}} Y(\mathbf{s}(t))$ are Gaussian processes on $\mathcal{T}$, $\Gamma^{(1)}(C_{t^*})$ and $\Gamma^{(2)}(C_{t^*})$ are valid *dependent* Gaussian processes on $\mathcal{T}$. Therefore, $\mathbf{\Gamma}(C_{t^*}) = (\Gamma^{(1)}(C_{t^*}), \Gamma^{(2)}(C_{t^*}))^\top \sim \mathcal{N}_2\big(\boldsymbol{\mu}_{\mathbf{\Gamma}}(t^*), \mathbf{K}_{\mathbf{\Gamma}}(t^*,t^*)\big)$, where $\boldsymbol{\mu}_{\mathbf{\Gamma}}(t^*) = \Big(\int_0^{t^*} D^{(1)}_{\mathbf{n}}\mu(\mathbf{s}(t))||\mathbf{s}'(t)||\,dt\,, \int_0^{t^*} D^{(2)}_{\mathbf{n},\mathbf{n}}\mu(\mathbf{s}(t))||\mathbf{s}'(t)||\,dt\Big)^\top = (m_1(t^*), m_2(t^*))^\top$ and $\mathbf{K}_{\mathbf{\Gamma}}(t^*,t^*) = \{k_{ij}(t^*,t^*)\}_{i,j=1,2}$ whose elements are evaluated as

$$k_{ij}(t^*,t^*) = (-1)^j \int_0^{t^*}\int_0^{t^*} \mathbf{a}_i^\top(t_1)\nabla^{i+j}K(\Delta(t_1,t_2))\,\mathbf{a}_j(t_2)||\mathbf{s}'(t_1)||||\mathbf{s}'(t_2)||\,dt_1\,dt_2\,, \tag{10}$$

where $\mathbf{a}_1(t) = \mathbf{n}(\mathbf{s}(t))$ and $\mathbf{a}_2(t) = \mathbf{c}_{\mathbf{n}(\mathbf{s}(t)),\mathbf{n}(\mathbf{s}(t))}$. Simplifications arise in $d = 2$. For example, $\mathbf{c}_{\mathbf{n},\mathbf{n}}(t) = (s_2'(t)^2, -2s_2'(t)s_1'(t), s_1'(t)^2)^\top$, while $\nabla^k K$, for $k = 2,3,4$, are matrices of orders 2×2, 2×3 and 3×3, respectively, of partial and mixed second, third and fourth derivatives of K and $\Delta(t_1,t_2) = \mathbf{s}(t_2) - \mathbf{s}(t_1)$. For any two points $t_1^*, t_2^* \in \mathcal{T}$, the dependence is specified through $\begin{pmatrix}\mathbf{\Gamma}(C_{t_1^*})\\ \mathbf{\Gamma}(C_{t_2^*})\end{pmatrix} \sim \mathcal{N}_4\left(\begin{pmatrix}\mathbf{m}_1\\ \mathbf{m}_2\end{pmatrix}, \begin{pmatrix}\mathbf{k}_{11} & \mathbf{k}_{12}\\ \mathbf{k}_{21} & \mathbf{k}_{22}\end{pmatrix}\right)$, where $\mathbf{m}_i = (m_i(t_1^*), m_i(t_2^*))^\top$, $\mathbf{k}_{ij} = \begin{pmatrix}k_{ij}(t_1^*,t_1^*) & k_{ij}(t_1^*,t_2^*)\\ k_{ij}(t_2^*,t_1^*) & k_{ij}(t_2^*,t_2^*)\end{pmatrix}$, $i,j = 1,2$. Generally, for n_P points partitioning $\mathcal{T}$ the above can be analogously extended. Clearly, $\mathbf{\Gamma}(C_{t^*})$ is a mean squared continuous process. However, stationarity of $Y(\mathbf{s})$ does not imply stationarity of $\mathbf{\Gamma}(C_{t^*})$. For any $\mathbf{s}_j \in \mathcal{S}$ with $\mathrm{cov}(Y(\mathbf{s}_j), \mathbf{\Gamma}(C_{t^*})) = \boldsymbol{\gamma}_j(t^*)$ and $\Delta_j(t) = \mathbf{s}(t) - \mathbf{s}_j$ we have,

$$\boldsymbol{\gamma}_j(t^*) = \left(\int_0^{t^*} D^{(1)}_{\mathbf{n}} K(\Delta_j(t))||\mathbf{s}'(t)||\,dt, \int_0^{t^*} D^{(2)}_{\mathbf{n},\mathbf{n}} K(\Delta_j(t))||\mathbf{s}'(t)||\,dt\right)^\top. \tag{11}$$

A valid *joint distribution* can be specified over $\mathcal{T}$ by,

$$\begin{pmatrix}\mathbf{Y}\\ \mathbf{\Gamma}(C_{t^*})\end{pmatrix} \sim \mathcal{N}_{L+2}\left(\begin{pmatrix}\boldsymbol{\mu}\\ \boldsymbol{\mu}_{\mathbf{\Gamma}}(t^*)\end{pmatrix}, \begin{pmatrix}\Sigma_{\mathbf{Y}} & \boldsymbol{\gamma}_{\mathbf{\Gamma}}(t^*)\\ \boldsymbol{\gamma}_{\mathbf{\Gamma}}^\top(t^*) & \mathbf{K}_{\mathbf{\Gamma}}(t^*,t^*)\end{pmatrix}\right), \tag{12}$$

where $\boldsymbol{\gamma}_{\mathbf{\Gamma}}^\top(t^*) = \big[\boldsymbol{\gamma}_1(t^*)\ \boldsymbol{\gamma}_2(t^*)\ \ldots\ \boldsymbol{\gamma}_L(t^*)\big]$ is the $2\times L$ cross-covariance matrix.

In practical applications curvilinear wombling is performed by approximating the curve C using linear segments. These measures at the segment level are then aggregated to produce a wombling measure for the curve. The curve is segmented using a partition. Consequently, the accuracy of estimated wombling measures for the curve depend on the choice of partition. Figures S2 and S3 in the supplementary materials illustrate this concept. Explicitly, let C be a regular rectifiable curve and $[a,b] \subset \mathcal{T}$ be a compact interval. Let g be a uniformly continuous function. For any partition, P of $[a,b]$, $a = t_0' < t_1' < \cdots < t_{n_P}' = b$, with its norm defined as $|P| = \max_{i=1,\ldots,n_P}(t_i' - t_{i-1}')$. A polygonal (piecewise-linear) approximation to the curve is, $\widetilde{C}_P = \bigcup_{i=1}^{n_P} C_{t_i}$, where $C_{t_i} = \{\mathbf{s}(t_{i-1}') + t\mathbf{u}_i, t \in [0,t_i]\}$, $t_i = ||\mathbf{s}(t_i') - \mathbf{s}(t_{i-1}')||$ and $\mathbf{u}_i = ||\mathbf{s}(t_i') - \mathbf{s}(t_{i-1}')||^{-1}(\mathbf{s}(t_i') - \mathbf{s}(t_{i-1}'))^\top$. Note that $\mathbf{s}(t) = \mathbf{s}(t_{i-1}') + t\mathbf{u}_i$ for $t \in [0,t_i]$ and, hence, $||\mathbf{s}'(t)|| = ||\mathbf{u}_i|| = 1$. Wombling measure for $\widetilde{C}_P$ is, $\Gamma(\widetilde{C}_P) = \sum_{i=1}^{n_P}\int_{C_{t_i}} g\left(\mathcal{L}Y(\mathbf{s}(t))\right)||\mathbf{s}'(t)||\,dt$. As $|P| \to 0$ we have, $\Gamma(\widetilde{C}_P) \xrightarrow{a.s.} \Gamma(C) = \int_a^b g\left(\mathcal{L}Y(\mathbf{s}(t))\right)||\mathbf{s}'(t)||\,dt$. This provides us with an estimate, $\Gamma(\widetilde{C}_P)$ for curvilinear wombling measures associated with any general curve C. Further details are provided in the supplementary materials, at the end of Section S5.

The choices of g for our wombling measures result in, $\mathbf{u}^\top\nabla Y$ and $\mathbf{c}_{\mathbf{u},\mathbf{u}}^\top \mathrm{vech}(\nabla^2 Y)$, which are linear and therefore uniformly continuous over any compact interval. Since predictive inference is performed iteratively on individual line segments, it is sufficient to show the inferential procedure for an arbitrary curve segment C_{t_i}. The normal to C_{t_i} is free of t and denoted as, $\mathbf{u}_i^\perp$, which is the normal to $\mathbf{u}_i$. The associated wombling measures with C_{t_i} are $\mathbf{\Gamma}(t_i) = \left(\int_0^{t_i} D^{(1)}_{\mathbf{u}_i^\perp} Y(\mathbf{s}(t))\,dt, \int_0^{t_i} D^{(2)}_{\mathbf{u}_i^\perp,\mathbf{u}_i^\perp} Y(\mathbf{s}(t))\,dt\right)^\top$. For a point $\mathbf{s}_j$ define $\Delta_{i-1,j} = \mathbf{s}_{i-1} - \mathbf{s}_j$, $j = 1,2,\ldots,L$. Their joint distribution is specified by (12), where $\boldsymbol{\gamma}_j(t_i)$ is obtained from (11) by replacing $\Delta_j(t)$ with $\Delta_{i-1,j} + t\mathbf{u}_i$ and $\mathbf{K}_{\mathbf{\Gamma}}(t_i,t_i)$ is obtained from (10) replacing $\Delta(t_1,t_2) = (t_2 - t_1)\mathbf{u}_i$ in the integrand. The analytic tractability of the line integrals in $\boldsymbol{\gamma}_j(t_i)$ is not a concern. Given choices of $\mu(\cdot)$ and $K(\cdot)$, they are all one or two dimensional integrals which are efficiently computed using simple quadrature. For example, let $Y(\mathbf{s})$ be the isotropic Gaussian process with mean $\mu(\mathbf{s}) = \mu$ and $K(||\Delta||;\sigma^2,\phi) = \sigma^2\exp(-\phi||\Delta||^2)$, where $\Delta = (\delta_1,\delta_2)^\top$. $\nabla^k K(\Delta)$, $k = 2,3,4$ is obtained from (2) and related results. $\boldsymbol{\gamma}_j(t_i) = \boldsymbol{\gamma}_j(t_i;\sigma^2,\phi) = \left\{\Phi\left(\sqrt{2\phi}\,(t_i + \mathbf{u}_i^\top\Delta_{i-1,j})\right) - \Phi\left(\sqrt{2\phi}\,\mathbf{u}_i^\top\Delta_{i-1,j}\right)\right\}(c_1,c_2)^\top$ where, $c_1 = c_1(\sigma^2,\phi,\mathbf{u}_i^\perp,\Delta_{i-1,j}) = -2\sigma^2\sqrt{\pi\phi}\,\mathbf{u}_i^{\perp\top}\Delta_{i-1,j}\,e^{-\phi\left(\mathbf{u}_i^{\perp\top}\Delta_{i-1,j}\right)^2}$,

$c_2 = c_2(\sigma^2, \phi, \mathbf{u}_i^{\perp}, \Delta_{i-1,j}) = c_1(1 - 2\phi \mathbf{u}_i^{\perp\top} \Delta_{i-1,j} \Delta_{i-1,j}^{\top} \mathbf{u}_i^{\perp})$, and $\Phi(\cdot)$ denotes the standard Gaussian cumulative distribution function. These are simple computations with quadrature required only for computing $K_{\mathbf{\Gamma}}(t_i, t_i)$.

4. Bayesian Hierarchical Model

We operate under a Bayesian hierarchical model, which is specified as

$$Y(\mathbf{s}) = \mu(\mathbf{s}, \boldsymbol{\beta}) + Z(\mathbf{s}) + \epsilon(\mathbf{s}) \,, \tag{13}$$

where $Z(\mathbf{s}) \sim \text{GP}(0, K(\cdot; \sigma^2, \phi))$ is a Gaussian process, and $\epsilon(\mathbf{s}) \sim N(0, \tau^2)$ is a white noise process, termed as the nugget (see Banerjee, Carlin, and Gelfand 2014, and references therein). The process parameters are $\boldsymbol{\theta} = \{\boldsymbol{\beta}, \sigma^2, \phi, \tau^2\}$. More generally, we can consider a latent specification for response arising from exponential families, $\alpha(\boldsymbol{\eta}(\mathbf{s})) = \mathbf{x}^{\top}(\mathbf{s})\boldsymbol{\beta} + Z(\mathbf{s}) + \epsilon(\mathbf{s})$, $Z(\mathbf{s}) \sim \text{GP}(0, K(\cdot; \sigma^2, \phi))$ and $Y(\mathbf{s}) \sim \pi(\boldsymbol{\eta}(\mathbf{s}), \cdot)$, where α is a monotonic link function, π is a member of the exponential family and $\boldsymbol{\eta}$ is the natural parameter. Predictive inference on differential processes and curvature wombling proceeds on the latent surface through $P(\mathcal{L}Z \mid \mathbf{Y})$. The joint posterior for differential processes is obtained through, $P(\nabla Z^{\top}, \text{vech}(\nabla^2 Z)^{\top} \mid \mathbf{Y}) = \int P(\nabla Z^{\top}, \text{vech}(\nabla^2 Z)^{\top} \mid \mathbf{Z}, \boldsymbol{\theta}) P(\mathbf{Z} \mid \mathbf{Y}, \boldsymbol{\theta}) P(\boldsymbol{\theta} \mid \mathbf{Y})\, d\boldsymbol{\theta}\, d\mathbf{Z}$, while wombling measures $\mathbf{\Gamma}_Z(t^*)$ for a curve C_{t^*} within the estimated posterior surface for $\mathbf{Z}$, are sampled from the posterior, $P(\mathbf{\Gamma}_Z(t^*) \mid \mathbf{Y}) = \int P(\mathbf{\Gamma}_Z(t^*) \mid \mathbf{Z}, \boldsymbol{\theta}) P(\mathbf{Z} \mid \mathbf{Y}, \boldsymbol{\theta}) P(\boldsymbol{\theta} \mid \mathbf{Y})\, d\boldsymbol{\theta}\, d\mathbf{Z}$. Customary prior specifications for $\boldsymbol{\theta}$ yield

$$\begin{aligned} P(\boldsymbol{\theta}, \mathbf{Z} \mid \mathbf{Y}) \propto\; & U(\phi \mid a_\phi, b_\phi) \times \text{IG}(\sigma^2 \mid a_\sigma, b_\sigma) \times \text{IG}(\tau^2 \mid a_\tau, b_\tau) \\ & \times \mathcal{N}_L(\mathbf{Z} \mid \mathbf{0}, \sigma^2 \mathbf{R}_Z) \times \mathcal{N}_p(\boldsymbol{\beta} \mid \mu_\beta, \Sigma_\beta) \\ & \times \prod_{l=1}^{L} \mathcal{N}_1\big(Y(\mathbf{s}_l) \mid \mathbf{x}(\mathbf{s}_l)^{\top}\boldsymbol{\beta} + Z(\mathbf{s}_l), \tau^2\big) \,, \end{aligned} \tag{14}$$

where IG denotes the inverse-gamma distribution with a shape-rate parameterization, U is a uniform distribution and $\mathbf{R}_Z$ is the correlation matrix corresponding to $K(\cdot; \sigma^2, \phi)$. The resulting full conditionals are $\boldsymbol{\beta} \mid \tau^2, \mathbf{Z}, \mathbf{Y} \sim \mathcal{N}_p(M_\beta m_\beta, M_\beta)$, $\sigma^2 \mid \phi, \mathbf{Z} \sim \text{IG}(a_\sigma + \frac{L}{2}, b_\sigma + \frac{1}{2}\mathbf{Z}^{\top}\mathbf{R}_Z^{-1}(\cdot;\phi)\mathbf{Z})$, $\tau^2 \mid \boldsymbol{\beta}, \mathbf{Z}, \mathbf{Y} \sim \text{IG}\left(a_\tau + \frac{L}{2}, b_\tau + \frac{1}{2}||\mathbf{Y} - \mathbf{X}\boldsymbol{\beta} - \mathbf{Z}||_2^2\right)$, $\mathbf{Z} \mid \mathbf{Y}, \boldsymbol{\theta} \sim \mathcal{N}_L(M_Z m_Z, \tau^2 M_Z)$, where $\mathbf{X}$ is the $L \times p$ matrix with $\mathbf{x}(\mathbf{s}_i)^{\top}$ as rows, $M_\beta^{-1} = \Sigma_\beta^{-1} + \tau^{-2}\mathbf{X}^{\top}\mathbf{X}$, $m_\beta = \Sigma_\beta^{-1}\mu_\beta + \tau^{-2}\mathbf{X}^{\top}(\mathbf{Y} - \mathbf{Z})$, $M_Z^{-1} = \tau^{-2}\big(\tau^{-2} I_L + \sigma^{-2}\mathbf{R}_Z^{-1}(\cdot;\phi)\big)$, and $m_Z = \mathbf{Y} - \mathbf{X}\boldsymbol{\beta}$. ϕ is updated using Metropolis steps with a normal proposal and an adaptive variance.

Under this setup posterior samples for the differential processes and wombling measures result from (5) and (6). For each posterior sample of $\{\mathbf{Z}, \boldsymbol{\theta}\}$, we draw $\mathbf{\Gamma}_Z(t^*) \mid \mathbf{Z}, \boldsymbol{\theta} \sim \mathcal{N}_2\big(\mu_{\mathbf{\Gamma}_Z}(t^*) - \boldsymbol{\gamma}_{\mathbf{\Gamma}_Z}^{\top}(t^*)\Sigma_{\mathbf{Z}}^{-1}\mathbf{Z}, K_{\mathbf{\Gamma}_Z}(t^*, t^*) - \boldsymbol{\gamma}_{\mathbf{\Gamma}_Z}^{\top}(t^*)\Sigma_{\mathbf{Z}}^{-1}\boldsymbol{\gamma}_{\mathbf{\Gamma}_Z}(t^*)\big)$, where $\mu_{\mathbf{\Gamma}_Z}(t^*)$, $\boldsymbol{\gamma}_{\mathbf{\Gamma}_Z}(t^*)$, and $K_{\mathbf{\Gamma}_Z}(t^*, t^*)$ are computed from (10) and (11). Algorithms 1 and 2 in the Supplement, Section S4, present further details for posterior sampling. Next, we turn to numerical experiments and data analyses. Codes required for reproducing and emulating the analyses presented in the manuscript are produced for the R statistical programming environment and available for download at *https://github.com/arh926/spWombling*.

5. Simulation Experiments

5.1. Data Generation

The proposed differential processes are not observed in reality, but are induced by an observed spatially indexed parent process. To evaluate statistical learning of the curvature process we perform simulation experiments within a setup where true values of the differential process and wombling measures are available. We consider locations $\mathbf{s} = (s_1, s_2)^{\top} \in \mathbb{R}^2$ over the unit square $[0, 1] \times [0, 1] \subset \mathbb{R}^2$. We generate synthetic data from two distributions: (a) Pattern 1: $y_1(\mathbf{s}) \sim N(10[\sin(3\pi s_1) + \cos(3\pi s_2)], \tau^2)$; (b) Pattern 2: $y_2(\mathbf{s}) \sim N(10[\sin(3\pi s_1) \cdot \cos(3\pi s_2)], \tau^2)$, where the value of $\tau^2 = 1$. Figure 1 presents spatial plots of the generated synthetic response from these patterns. The rationale behind selecting these distributions is: (i) synthetic data is more practical and not from the model in (13), and (ii) true gradient and curvature can be computed at every location $\mathbf{s}$.

The synthetic patterns chosen feature two different scenarios that may arise. In the first pattern expressions for differentials along the principal directions $\mathbf{e}_1 = (1, 0)^{\top}$ and $\mathbf{e}_2 = (0, 1)^{\top}$ are functions of either s_1 or s_2, $\nabla\mu_1(\mathbf{s}) = 30\pi(\cos(3\pi s_1), -\sin(3\pi s_2))^{\top}$, $\nabla^2\mu_1(\mathbf{s}) = -90\pi^2 \text{diag}\{\sin(3\pi s_1), \cos(3\pi s_2)\}$. The curvature along s_1 does not influence curvature along s_2, $\big(\nabla^2\mu_1(\mathbf{s})\big)_{12} = 0$ for all $\mathbf{s}$. While $\nabla\mu_2(\mathbf{s}) = 30\pi(\cos(3\pi s_1)\cos(3\pi s_2), -\sin(3\pi s_1)\sin(3\pi s_2))^{\top}$, $\nabla^2\mu_2(\mathbf{s}) = -90\pi^2 M(\mathbf{s})$, where $M(\mathbf{s})$ is a 2×2 matrix with, $m_{11} = \sin(3\pi s_1)\cos(3\pi s_2)$, $m_{12} = m_{21} = \cos(3\pi s_1)\sin(3\pi s_2)$ and $m_{22} = \sin(3\pi s_1)\cos(3\pi s_2)$ with differentials being functions of

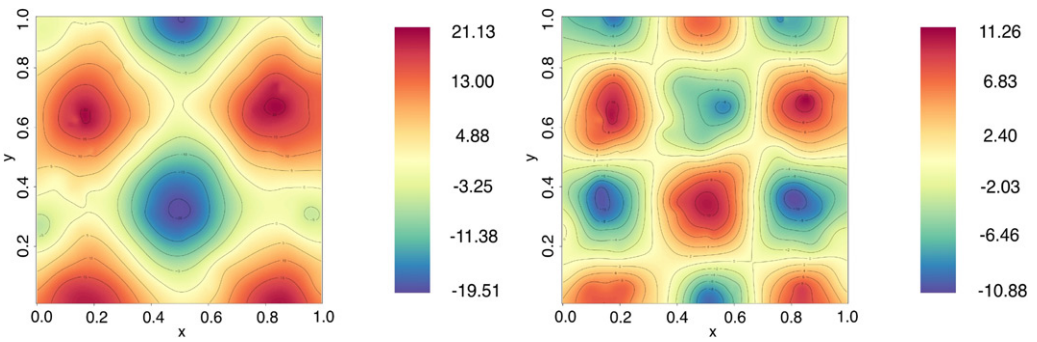

Figure 1. Spatial plots for synthetic patterns, from Pattern 1 (left) and Pattern 2 (right). Scales are shown in the legend alongside.

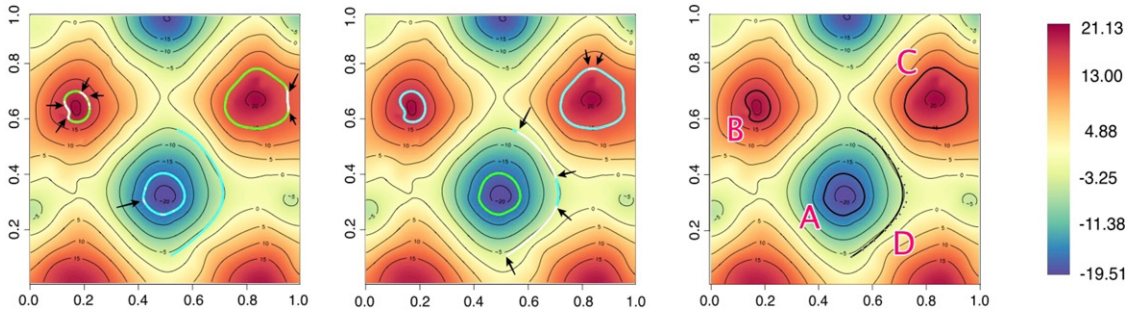

Figure 2. (left) shows color coded directional gradients for segments, (center) shows color coded directional curvature for segments in the direction normal to the curve, (right) shows curves selected for performing curvature wombling. `green` indicates a positive significance, `cyan` indicates negative significance and `white` indicates no significance.

both s_1 and s_2 and $\left(\nabla^2\mu(\mathbf{s})\right)_{12} \neq 0$ for some $\mathbf{s}$. While setting up the experiments we vary $L \in \{100, 500, 1000\}$ with 10 replicated instances under each setting.

5.2. Bayesian Model Fitting

We fit the model in (14) with only an intercept allowing the spatial process to learn the functional patterns in the synthetic response. We use the following hyperparameter values in (14): $a_\phi = 3/\max||\Delta||$, $b_\phi = 30$, $a_\sigma = 2$, $b_\sigma = 1$, $a_\tau = 2$, $b_\tau = 0.1$ $\mu_\beta = 0$ and $\Sigma_\beta = 10^6 I_p$. These choices comprise reasonable weakly informative priors. While a Uniform(2, 3) prior on ν can be specified (and was implemented as part of this experiment) to ensure the existence of the curvature process, here our choice of scales in the data-generating patterns ensured that $\nu = 5/2$ provided the best model fit when compared with values of $\nu \in \{1/2, 3/2, 5/2\}$. Hence, we present the results with $\nu = 5/2$.

The parameter estimates for $\boldsymbol{\theta}$ are computed using posterior medians and their highest posterior density (HPD) intervals (Chen and Shao 1999; Plummer et al. 2015). For each replicate, we assess our ability to estimate the local geometry of the resulting posterior surface. For this we overlay a grid spanning the unit square. We perform posterior predictive inference for the differential processes at each grid location following Section 2. Posterior predictive medians (accompanied by 95% HPD intervals) summarize inference for the differential processes over the grid locations (Section 5.4 offers supplementary analysis).

5.3. Bayesian Wombling with Curvature Processes

For wombling with curvature processes, or *curvature wombling*, we focus on locating curves that track rapid change within the simulated random surfaces. For example, consider the surface produced by the first pattern. If a curve is provided to us, we can evaluate the posterior distribution of the average or total curvature wombling measures to assess their statistical significance. On the other hand, without a given curve, we consider three different approaches for constructing them from a boundary analysis or wombling perspective: (a) level curves: $C_{y_0} = \{\mathbf{s} : Y(\mathbf{s}) = y_0\}$: Bayesian wombling literature finds that curves parallel to contours often form wombling boundaries (see, e.g., Banerjee and Gelfand 2006) and level curves on a surface are parallel to local contours by definition; (b) smooth curves: produces a smooth curve using Bézier splines (see, e.g., Gallier and Gallier 2000) from a set of *annotated* points that are of interest within the surface; and (c) rectilinear curves: produces a rectilinear curve joining adjacent *annotated* points of interest within the surface using straight lines, performs curvature wombling using a Riemann sum approximation (see (S1) in the supplementary materials). Curves of types (b) and (c) allow the investigator to specify a region of interest that house possible wombling boundaries. For the surface realization produced by Pattern 1, we consider four different types of curves on the response surface, (A) a closed curve enclosing a trough corresponding to a level curve, $C_{y_0=-18}$, (B) a closed curve enclosing a peak corresponding to a level curve, $C_{y_0=+18}$, (C) a closed curve that outlines a contour corresponding to a level curve, $C_{y_0=+15}$ and (D) an open curve along a contour constructed using a Bézier spline. These curves are marked in Figure 2(right).

Curvature wombling is performed using methods outlined in Section 3. Referring to the discussion on rectilinear approximation, for each curve, given a partition, we compute t_i and $\mathbf{u}_i$. Combining the segments produces a vector $\mathbf{t}$ and a matrix of directions, $\mathbf{U}$ that represents the curve. Algorithm 2 in the Section S4, supplementary materials devises efficient computation using $\mathbf{t}$ and $\mathbf{U}$. The total (and average) wombling measures $\overline{\boldsymbol{\Gamma}}(C)$ are sampled from their posteriors using (12). For curves A, B, C and D, we use partitions with sufficiently small norms ($|P|$) to achieve accuracy (3.99×10^{-3}, 3.97×10^{-3}, 4.42×10^{-3} and 2.66×10^{-2}, respectively). One and two dimensional line integrals (refer to (10) and (11)) are computed via quadrature using grids of size 10 on $[0, t_i]$, and size 100 on $[0, t_i] \times [0, t_i]$, respectively, for $i = 1, 2, \ldots, n_P$. The median of sampled $\overline{\boldsymbol{\Gamma}}(\widetilde{C}_P)$ is our estimated wombling measure for the curve. Significance at the curve-segment level is assessed based on the inclusion of 0 within the HPD intervals. Our design allows us to compute true values of average wombling measures for each rectilinear segment in the curve. They are computed using, $\mu_{\boldsymbol{\Gamma}}^{\text{true}}(\widetilde{C}_P) = \left(\sum_{i=1}^{n_P} t_i\right)^{-1}\left(\sum_{i=1}^{n_P}\int_0^{t_i} \mathbf{u}_i^{\perp\top}\nabla\mu_1(\mathbf{s}(t))\,dt, \sum_{i=1}^{n_P}\int_0^{t_i} \mathbf{u}_i^{\perp\top}\nabla^2\mu_1(\mathbf{s}(t))\mathbf{u}_i^{\perp}\,dt\right)^\top$. We compute HPD intervals for the wombling measures at the segment level. Coverage probabilities (CPs) are then constructed by aggregating coverage of true values by HPD intervals over segments.

Curve A encloses a trough and a local minima for the surface, while B and C enclose peaks and local maximums (referring to corresponding locations in Figures S8c and S9c). Along all segments of A we expect negative gradients owing to the decreasing

Table 1. Results from curvature wombling performed on curves A, B, C, and D as shown in Figure 2.

Curves (C)	Average gradient ($\Gamma^{(1)}(C)$)		Average curvature ($\Gamma^{(2)}(C)$)	
	True	Estimated	True	Estimated
Curve A	−61.54	−64.97 (−92.37, −38.57)	731.94	768.03 (599.30, 913.70)
Curve B	40.85	49.19 (20.45, 73.12)	−808.04	-850.84 (−1066.98, −630.09)
Curve C	84.03	85.65 (59.81, 109.97)	−558.58	-504.98 (−767.55, −241.61)
Curve D	−110.84	−113.27 (−153.23, −77.01)	11.32	**−94.64 (−386.94, 233.78)**

NOTE: The estimated average directional gradient and curvature are accompanied by their respective HPD intervals in brackets. HPD intervals *containing 0* are marked in bold.

nature of the response in that region, while for B and C we expect positive gradients. Each of them would be expected to yield significant wombling measures for gradients. Referring to the Laplacian surface (see Figures S8e and S9e) A, B, and C are located in regions manifesting rapid change in the gradient surface, implying they should yield large positive (curve A) or negative (curves B and C) curvature, forming curvature wombling boundaries. These are all aligned with our findings presented in Table 1, which presents measures of quality assessment for wombling. The magnitude and sign of wombling measures also allow us to differentiate between the type of curvature for the different wombling boundaries. For instance, B is located in a region of higher convexity compared to C, while the nature of convexity for regions enclosed by them are different compared to A. Plots in Figure 2 (left and center) show line segment level inference for average wombling measures. Arrows indicate segments which were not significant with respect to gradient or curvature, while regions of significance are color coded. D is located in a "relatively flat" region of the surface (see Figures S8e and S9e) and is expected to have gradients but no curvature, which aligns with results shown in Table 1. We conclude by noting that the true values, $\mu_{\Gamma}^{\text{true}}(C)$ of the wombling measures for the curves considered, are all covered by the estimated HPD intervals for respective curves. Additionally, at the line segment level we achieved a CP of 1.0 across all curves.

5.4. Supplementary Analysis

We present additional results in the online supplement. Tables S1 and S2 present parameter estimates, measures of goodness of fit for the fitted process, and assessment of derivative process characteristics for each pattern considered. We compute root mean square errors (RMSE) across observed locations averaged over 10 replicates for each sample size setting for the fitted process $\widehat{Y}(\mathbf{s}) = \widehat{\beta}_0 + \widehat{Z}(\mathbf{s})$, and $\widehat{\nabla Y(\mathbf{s})}$, $\widehat{\text{vech}(\nabla^2 Y(\mathbf{s}))}$. We report standard deviations across replicates. With increasing number of observed locations we are able to effectively learn the underlying process and induced differential processes. Figures S4–S7 present spatial plots of posterior medians of gradient and curvature processes, for $L = 100$ locations. These plots demonstrate the effectiveness of our methods in learning about the differential processes from the underlying patterns. Similarly plots shown in Figures S8–S11 demonstrate the same for derived quantities and operators of $\mathcal{L}Y(\mathbf{s})$—principal curvature (eigenvalues), Gaussian curvature (determinant) (see, e.g., Spivak 1999; Do Carmo 2016), divergence and Laplacian, which pertain to geometric analysis of curvature for the random surface resulting from the underlying patterns. Statistical significance is assessed at every grid point by checking the inclusion of 0 in their HPD intervals. Significantly positive (negative) points are color coded. We compute average CPs at every grid location to measure the accuracy of our assessment. These CPs are then averaged over replicates. We observed high CPs across the grid for parent and differential processes. Figures S12 and S13 compare observed against estimated differential processes coupled with their HPD regions.

6. Applications

Frameworks developed for differential assessment and boundary analysis in spatially indexed response are applied to multiple datasets with the aim of locating curvature wombling boundaries that track rapid change in response. The chosen data arise from varied areas of scientific interest, we briefly describe the origin and significance of each with respect to our methods before performing our analysis. Response is modeled using the hierarchical model in (13). Prior specifications used in (14) are, $\phi \sim \text{Unif}\,(3/\max_{\mathbf{s}\in\mathcal{S}}||\Delta||, 300)$, $\sigma^2 \sim \text{IG}(2,1)$, $\tau^2 \sim \text{IG}(2,1)$ (mean 1, infinite variance), $\boldsymbol{\beta} \sim N(0, 10^6 I_p)$, p being the number of covariates and $\nu = 5/2$ for the Matérn kernel ensuring existence of the differential processes.

Boston Housing: The Boston housing data (see, e.g., Harrison Jr and Rubinfeld 1978) was collected by the United States Census Service featuring median house prices for tracts and towns in Boston, Massachusetts area. The purpose was to study heterogeneity in the market caused by the need for residents to have clean air. To study such heterogeneity, modern equitable housing policies are incorporating statistical modeling to quantify such behavior. Often they are a result of unobserved effects of rapidly shifting socioeconomic conditions (see, e.g., Hu et al. 2019). Within a spatial map this manifests as neighboring regions of disparity. Figure 3 shows two such regions: high priced including Downtown Boston, Cambridge, Newton, Wellesley, Brookline etc. and low priced including South and East End. For effective policy implementation, identifying such regions becomes crucial. Spatial variation in the median house prices is evidenced in Figure 4. Curvature wombling effected on the house price surface would locate regions that feature such change.

The data contains median house price values for 506 census-tracts along with demographic data. Latitude-longitude centers of the census-tracts are used for spatial referencing. To allow $Z(\mathbf{s})$ to capture all the spatial variation, we include only an intercept in the model. Table 2 shows posterior estimates and HPD intervals for process parameters. We observe that $\frac{\sigma^2}{\sigma^2+\tau^2} \approx$ 78.75%—larger portion of total variance being explained by varying location.

Modeled spatial variation in the response is shown in Figure 3 (left). Significance for the estimate, $\widehat{Z}(\mathbf{s})$, is assessed using the inclusion of 0 in its posterior HPD. Using posterior samples we estimate the derivative processes for $Z(\mathbf{s})$. A grid, $(\mathcal{G} = \{\mathbf{s}_g : \mathbf{s}_g \in \texttt{convex-hull}(\mathcal{S})\}$, containing 1229 equally

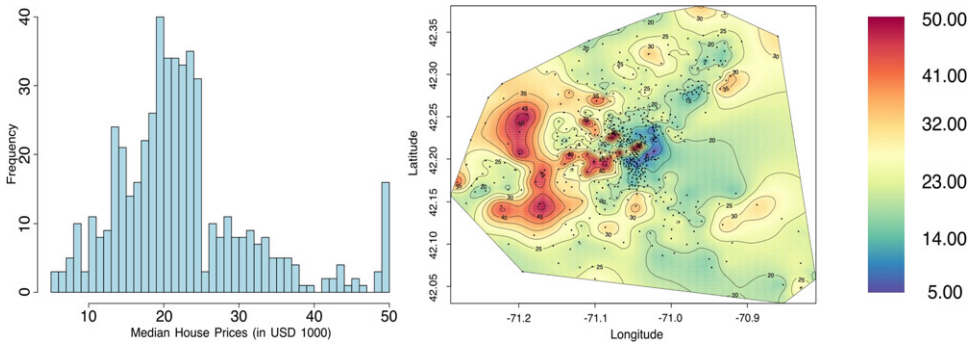

Figure 3. Plots showing (left) probability density of median house prices (in USD 1000) (right) spatial plot of median owner occupied house prices in Boston.

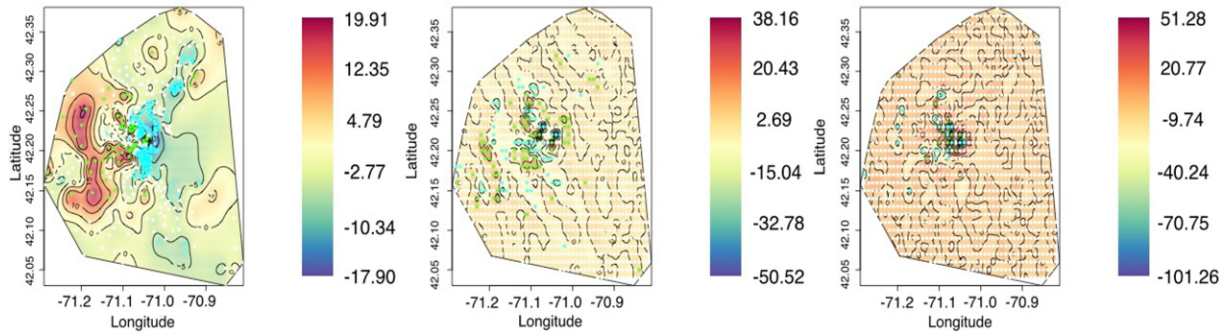

Figure 4. Plots (left to right) showing fitted process, divergence and Laplacian for the median house price surface.

Table 2. Posterior Estimates from the hierarchical linear model in (13) to Boston housing.

Parameters ($\boldsymbol{\theta}$)	Posterior estimates ($\widehat{\boldsymbol{\theta}}$)	HPD
ϕ	0.96	(0.83, 1.11)
σ^2	55.18	(43.91, 68.06)
τ^2	14.89	(11.77, 18.71)
β_0	25.58	(24.29, 27.34)

Table 3. Curvature wombling measures for boundaries in Boston housing accompanied by corresponding HPD intervals in brackets below.

Curve (C)	Average gradient ($\overline{\Gamma}^{(1)}(C)$)	Average curvature ($\overline{\Gamma}^{(2)}(C)$)
Boundary 1	−8.91	10.14
	(−11.31, −6.65)	(2.84, 18.34)
Boundary 2	6.18	**−0.09**
	(4.75, 7.49)	**(−3.45, 3.35)**
Boundary 3	−6.47	12.69
	(−9.74, −3.27)	(2.65, 22.48)
Boundary 4	6.92	**1.26**
	(4.63, 9.19)	**(−5.04, 7.14)**
Boundary 5	5.47	**1.36**
	(2.95, 7.86)	**(−4.33, 7.42)**
Boundary 6	11.82	−16.27
	(7.28, 16.14)	(−26.68, −6.57)

NOTE: Estimates corresponding to HPD intervals containing 0 are marked in bold.

spaced locations) is overlaid over the region with the same purpose. To effect posterior surface analysis on the estimated surface we use posterior predictive distributions of div(Z) and $\Delta(Z)$ revealing zones that manifest rapid change in response and gradients, respectively. They are shown in Figures 4 (center and right). Next, we focus on performing curvature wombling on the estimated surface. Strategic posterior surface analysis is used to locate level-sets of interest within the surface that could possibly contain wombling boundaries. We start with contours shown in Figure 5 (left column). Boundary 1 (2) bounds a region where the fitted process has positive (negative) significant estimates. Evidently, the chosen curves should house significant gradients along most segments, but significant curvature should only be detected for segments located at the center (lat-long: $(42.18, 42.23) \times (-71.05, -70.05)$) of the surface in Figures 4 (center and right). Estimated average wombling measures for these curves are shown in Table 3. Figures 5 (center and right) correspond to segment level posterior inference for the curves, line segments with significant directional differentials are indicated in bold. Summarizing, we observe that the gradient, curvature and posterior surface analysis allow us to highlight towns (with census-tracts) within Boston that exhibit heterogeneity in prices. Curvature wombling performed on the surface allows us to delineate zones that house such heterogeneity. For instance, towns located within boundaries 3 (South and East End) and 6 (Newton and Brookline) show significant change in price gradients, compared to towns within boundaries 4 (Lincoln and Weston) and 5 (Wellesley and Dover). These findings can be verified referring back to price dynamics for real estate in Boston during 1978 (see, e.g., Schnare and Struyk 1976). The same regions are scrutinized for studying segmentation—towns within curves 1 and 3 are accessible to lower income groups willing to sacrifice air quality.

Meuse River Data: The Meuse river data features in Pebesma et al. (2012). It provides locations of topsoil heavy metal concentrations, along with soil and landscape variables at the observed locations, collected in a flood plain of the river Meuse, near the village of Stein, Netherlands. The heavy metal concentrations recorded include Cadmium (Cd), Copper (Cu), Lead (Pb), and

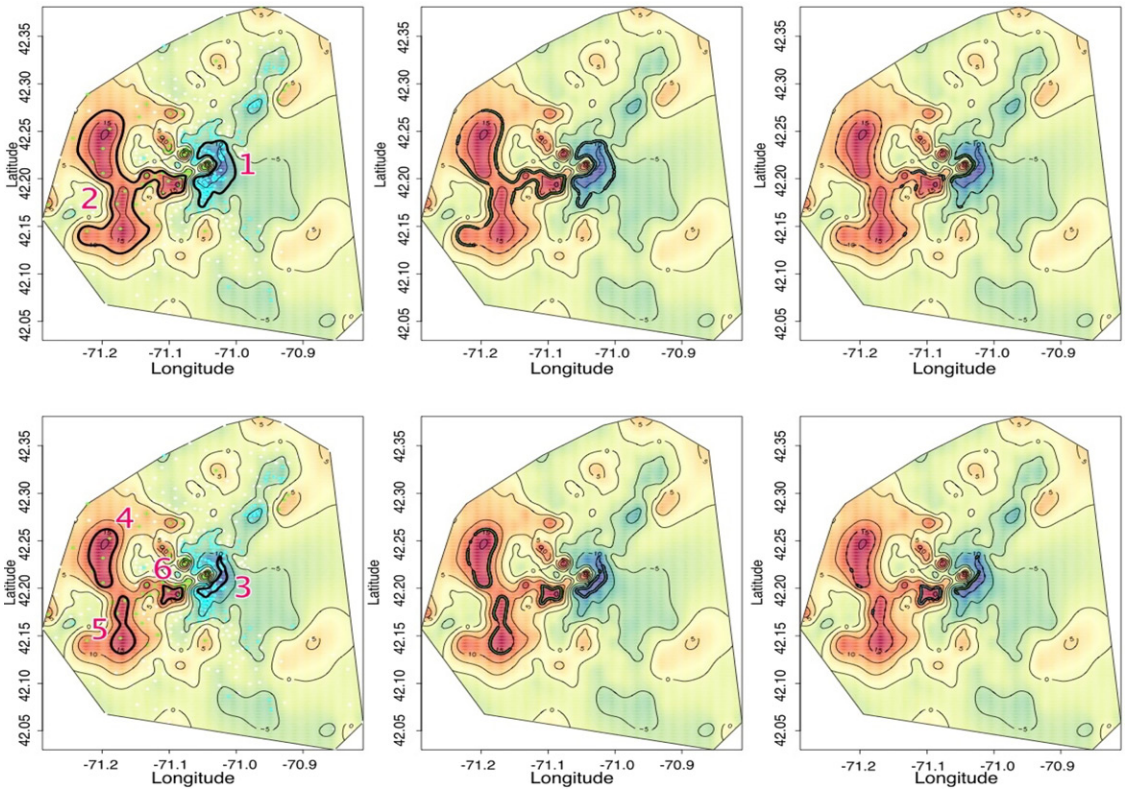

Figure 5. Curvature wombling on the Boston Housing Data.

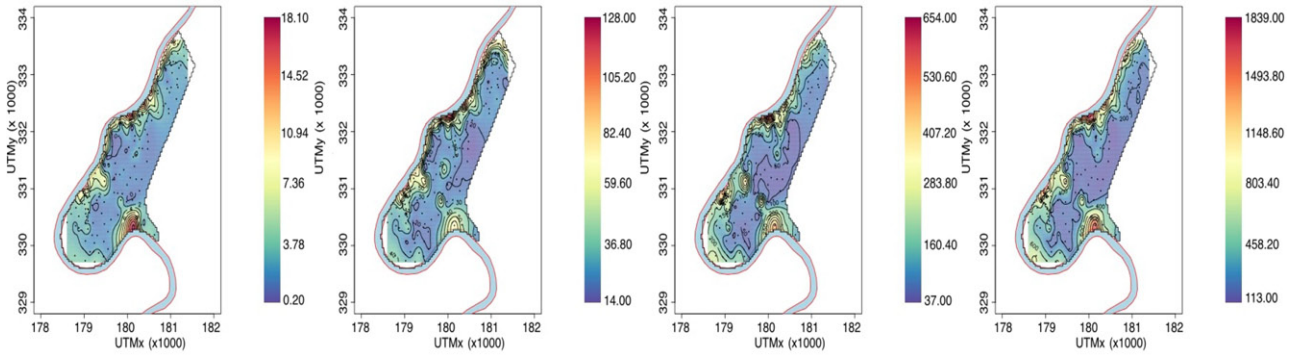

Figure 6. Plots showing heavy metal concentrations in the topsoil of a flood plain at 155 locations for (from left to right) Cadmium (Cd), Copper (Cu), Lead (Pb), and Zinc (Zn) (in mg/kg of soil).

Zinc (Zn). A distinguishing feature is the naturally occurring boundary—the Meuse. From a boundary analysis standpoint we are interested in examining differentials in heavy metal concentrations along the flood plain of the river to understand the heterogeneous effect of the river on the topsoil. The soils of the floodplain are commonly used for agriculture. Crops grown on the floodplain of the river banks of the Meuse may be consumed by man and/or livestock. The spatial variation in heavy metal concentration can be seen in Figure 6. The path of the Meuse river is shown in each of the spatial plots. Evidently, the heavy metal concentrations decreases with increasing distance from the river. We model the concentrations as independent Gaussian processes. Covariates used are relative elevation above local river bed (`elev`, measured in meters), organic matter (`om` measured in kg/(100kg) of soil), distance to Meuse (`dist`), frequency of flooding, soil type (`soil`), and lime content in soil ($p = 9$). Table 4 shows the posterior estimates of process parameters and model coefficients, $\boldsymbol{\beta}$ for each of the heavy metals in question. We observe that $\sigma^2/(\sigma^2 + \tau^2) \approx 62.45\%$, 99.79%, 52.09%, 62.29% for Cd, Cu, Pb, and Zn, respectively, indicating larger portions of total variation being explained by spatial heterogeneity, except for Pb. Variation in Cd and Zn concentration is significantly affected by elevation, organic matter and flooding frequency, while variations in Cu and Pb concentration is significantly affected by elevation, organic matter and flooding frequency and lime content. The estimated residual surface is shown in Figure 7 (left) for Cd concentrations. We observe significant positive gradients with varying curvature depending on segments of the river bed for all heavy metals. We perform curvature wombling on the Meuse using the residual surface, $\mathbf{Z}$. The results of curvature wombling for cadmium are shown in Figure 7. Results and plots for other metals can be found

Table 4. Posterior estimates of process parameters and covariates for the Meuse river data accompanied by their corresponding HPD intervals in brackets below.

Parameters ($\boldsymbol{\theta}$)	Cadmium (Cd)	Copper (Cu)	Lead (Pb)	Zinc (Zn)
ϕ	0.0379	0.1138	0.0399	0.0472
	(0.0207, 0.0618)	(0.0871, 0.1471)	(0.0131, 0.1900)	(0.0230, 0.0744)
σ^2	2.9566	3.2044	0.9303	38.3538
	(1.2803, 5.2227)	(2.3955, 4.0892)	(0.2763, 1.7641)	(16.7815, 65.1450)
τ^2	1.7771	0.0067	0.8555	23.2226
	(0.9107, 2.6328)	(0.0012, 0.0244)	(0.0010, 1.2280)	(9.3743, 35.6867)
`Intercept`	9.4973	4.8503	6.1120	37.1315
	(5.9750, 13.3704)	(3.1392, 6.8308)	(3.4615, 8.1910)	(25.0903, 53.0870)
`elev`	−0.7672	−0.4065	−0.5413	−2.8781
	(-1.2531, −0.3574)	(−0.7418, −0.1656)	(−0.7853, −0.1442)	(−4.7805, −1.2834)
`om`	0.4011	0.4293	0.3434	0.8606
	(0.2616, 0.5233)	(0.3276, 0.4728)	(0.2490, 0.4253)	(0.3681, 1.3166)
`dist`	**−0.0033**	**−0.0025**	**−0.0011**	**−0.0081**
	(−0.0061, 0.0000)	(−0.0043, −0.0014)	(−0.0029, 0.0006)	(−0.0197, 0.0038)
`ffreq (=2)`	−1.4176	−2.4727	−0.8483	−4.3182
	(−2.3202, −0.3432)	(−3.1794, −1.6716)	(−1.6109, −0.2598)	(−7.9184, −0.6220)
`ffreq (=3)`	**−0.7322**	−1.4298	**−0.1865**	**−3.3159**
	(−2.0520, 0.6248)	(−2.4443, −0.5157)	(−1.2972, 0.6861)	(−7.9307, 1.9128)
`soil (=2)`	**−0.3337**	**0.2236**	**0.5988**	**−2.2213**
	(−1.4661, 0.7491)	(−0.7248, 0.9799)	(−0.0345, 1.2956)	(−6.1446, 2.0831)
`soil (=3)`	**−0.3884**	**0.6344**	**0.3707**	**−2.9922**
	(−2.0891, 1.2628)	(−0.2309, 1.8474)	(−0.7108, 1.4029)	(−9.0918, 3.6289)
`lime (=1)`	**0.5752**	1.3223	0.7759	**−0.4759**
	(−0.3509, 1.4341)	(0.7152, 1.9427)	(0.1173, 1.4645)	(−3.9057, 2.6510)

NOTE: Effects with HPDs containing 0 are marked in bold.

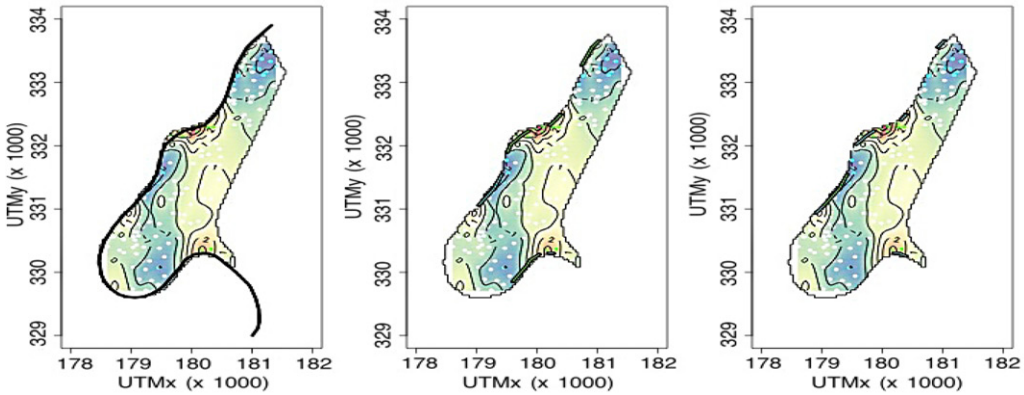

Figure 7. Plots showing results for curvature wombling on the Meuse river for Cadmium (Cd) concentration. Plots showing (left) the resulting fitted process (center) the contiguous segments that display significant gradients (right) the contiguous segments with significant curvature.

in the Section S7, Figure S14, supplementary materials. The accompanying wombling measures are shown in Table 5. We observe sufficient heterogeneity in the signs of the wombling measures, yielding contiguous positive (negative) segments. For example, in Cd concentration, boundaries located for average gradients in the northern and southern region are positive, as opposed to boundaries located in the north western region. Therefore, while displaying the wombling measures, in Table 5, we separate them by their sign.

We conclude that effects of river Meuse on regions of the flood plain exhibit significant heterogeneity when considered across heavy metals. Compared to other metals, Pb concentrations are limited to northern regions of the flood plain. Concentrations of Cd and Zn concentrations along the river are similar. Compared to the northern region, in the northwestern region Zn concentrations decrease significantly as we move inland. Studies corroborating such evidence can be found in Leenaers, Schouten, and Rang (1988) and Albering et al. (1999).

7. Discussion and Future Work

We developed a fully model-based Bayesian inferential framework for differential process assessment and curvature-based boundary analysis for spatial processes. Introducing the directional curvature process and its associated inferential framework supplements the directional gradients with inference for their rates of change, while its induction into the folds of Bayesian curvilinear wombling allows for further characterization of difference boundaries. Adopting a Bayesian hierarchical model allows for Gaussian calibration when characterizing points, regions and boundaries within a surface. This framework is widely applicable; our applications arise from selected disciplines indicating the utilities of mapping curvature process boundaries to understand spatial data-generating patterns. Substantive case studies will be reported separately.

Several avenues hold scope for future developments. A more generalized theoretical framework can be developed for studying joint behavior of the principal curvature (direction

Table 5. Curvature wombling measures for the Meuse, separated by zones of positive and negative signs, they are accompanied by their corresponding HPD intervals in brackets below.

Wombling Measures	Cd	Cu	Pb	Zn
$\overline{\Gamma}^{(1)}(>0)$	0.0510 (0.0298, 0.07401)	0.1273 (0.0913, 0.1729)	0.0375 (0.0019, 0.1561)	0.1984 (0.0876, 0.3162)
$\overline{\Gamma}^{(1)}(<0)$	−0.0400 (−0.0635, −0.0170)	−0.2561 (−0.3187, −0.1997)	– –	−0.1890 (-0.2967, -0.0669)
$\overline{\Gamma}^{(2)}(>0)$	0.0074 (0.0019, 0.0158)	– –	– –	0.0422 (0.0111, 0.0879)
$\overline{\Gamma}^{(2)}(<0)$	−0.0078 (−0.0223, −0.0024)	−0.1247 (−0.1979, −0.0860)	−0.0039 (−0.1076, −0.0006)	−0.0473 (−0.1114, −0.0095)

of maximum (or minimum) curvature) and the aspect (direction of maximum gradient) (see, e.g., Wang, Bhattacharya, and Gelfand 2018) leveraging dependent circular uniform distributions (see, e.g., Kent, Mardia, and Taylor 2008). We offer some brief remarks . To obtain the direction of maximum curvature for a spatial surface, we solve $\max_{\mathbf{u}\in\mathbb{R}^2} \left|\mathbf{u}^\top \nabla^2 Y(\mathbf{s})\mathbf{u}\right|$, such that $||\mathbf{u}|| = 1$, at an arbitrary point $\mathbf{s}$. Using Lagrange multipliers and denoting $\kappa(\mathbf{u}) = |\mathbf{u}^\top \nabla^2 Y(\mathbf{s})\mathbf{u}|$, define $\mathcal{O}(\mathbf{u}) = \kappa(\mathbf{u}) - \lambda(||\mathbf{u}||^2 - 1)$ hence, $\partial\mathcal{O}(\mathbf{u})/\partial u_i = \kappa(\mathbf{u})^{-1}(\nabla^2_{ii} Y(\mathbf{s})u_i + \nabla^2_{ij} Y(\mathbf{s})u_j) - \lambda u_i = 0$, $i,j = 1,2$. With $u_2/u_1 = \tan\theta_{pc}$, eliminating λ we get $\tan\theta_{pc} = \dfrac{\nabla^2_{22} Y(\mathbf{s}) \tan\theta_{pc} + \nabla^2_{12} Y(\mathbf{s})}{\nabla^2_{11} Y(\mathbf{s}) + \nabla^2_{12} Y(\mathbf{s}) \tan\theta_{pc}}$. Defining $h_1 = h_1(\mathbf{s}) = (\nabla^2_{11} Y(\mathbf{s}) - \nabla^2_{22} Y(\mathbf{s}))/\nabla^2_{12} Y(\mathbf{s})$ given $\nabla^2_{12} Y(\mathbf{s}) \neq 0$ and solving $\theta_{pc} = \tan^{-1}\frac{1}{2}\left[-h_1 \pm \sqrt{h_1^2 + 4}\right]$. If $\nabla^2_{12} Y(\mathbf{s}) = 0$ then, $\nabla^2 Y(\mathbf{s})$ is diagonal and θ_{pc} corresponds to the direction of $\max\{\nabla^2_{11} Y(\mathbf{s}), \nabla^2_{22} Y(\mathbf{s})\}$. We propose that $\Theta = (\theta_{asp}, \theta_{pc})^\top$ follows a dependent circular uniform distribution over $[0, 2\pi] \times [0, 2\pi]$. Further developments with circular regression methods can proceed to examine the effect of covariates on Θ. Multivariate extensions would involve formulating these differential processes on arbitrary manifolds. This requires simulating a Gaussian process on manifolds and inspecting the covariant derivative. Bayesian curvilinear wombling could then be implemented on curves of interest to the investigator. This would not only involve an inferential framework for normal curvature, but also geodesic curvature for such curves. Spatiotemporal curvature processes can build upon Quick, Banerjee, and Carlin (2015) to study evolutionary behavior of the curvature processes with respect to variations in the response across time. Finally, we remark that while there have been substantial recent developments in scalable spatial processes for massive datasets—a comprehensive review is beyond the scope of the current article (see, e.g., Heaton et al. 2019)—not all scalable processes admit the correct degree of smoothness for curvature processes to exist. Constructing scalable processes for curvilinear wombling, and subsequent inference, remains a problem of interest in the wombling community.

Supplementary Materials

The online supplement includes additional theoretical derivations and computational details on spatial curvature processes, additional simulation experiment results referenced in Section 5.4 and wombling for Northeastern US temperatures during January, 2000.

Acknowledgments

The authors thank the Editor, Associate Editor, and two anonymous reviewers for several helpful comments that improved the manuscript.

Funding

Sudipto Banerjee was supported, in part, by the National Science Foundation (NSF) through grants DMS-2113778 and DMS-1916349; and by the National Institute of Environmental Health Sciences (NIEHS) under grants R01ES030210 and R01ES027027

References

Abramowitz, M., Stegun, I. A., and Romer, R. H. (1988), *Handbook of Mathematical Functions with Formulas, Graphs, and Mathematical Tables*, Washington, DC: United States. Government Printing Office. [1157]

Adler, R. J. (1981), *The Geometry of Random Fields*, Philadelphia, PA: SIAM. [1155]

Albering, H. J., Van Leusen, S. M., Moonen, E., Hoogewerff, J. A., and Kleinjans, J. (1999), "Human Health Risk Assessment: A Case Study Involving Heavy Metal Soil Contamination After The Flooding of The River Meuse During The Winter Of 1993-1994," *Environmental Health Perspectives*, 107, 37–43. [1165]

Banerjee, S. (2010), "Spatial Gradients and Wombling," in *Handbook of Spatial Statistics*, eds. A. E. Gelfand, P. Diggle, P. Guttorp, and M. Fuentes, 559–574, Boca Raton, FL: Taylor and Francis/CRC. [1155]

Banerjee, S., Carlin, B. P., and Gelfand, A. E. (2014), *Hierarchical Modeling and Analysis for Spatial Data*, Boca Raton, FL: CRC Press. [1160]

Banerjee, S., and Gelfand, A. (2003), "On Smoothness Properties of Spatial Processes," *Journal of Multivariate Analysis*, 84, 85–100. [1155]

Banerjee, S., and Gelfand, A. E. (2006), "Bayesian Wombling: Curvilinear Gradient Assessment Under Spatial Process Models," *Journal of the American Statistical Association*, 101, 1487–1501. [1155,1156,1158,1159,1161]

Banerjee, S., Gelfand, A. E., and Sirmans, C. (2003), "Directional Rates of Change Under Spatial Process Models," *Journal of the American Statistical Association*, 98, 946–954. [1155,1157]

Burrough, P. A., McDonnell, R. A., and Lloyd, C. D. (2015), *Principles of Geographical Information Systems*, Oxford: Oxford University Press. [1155]

Chen, M.-H., and Shao, Q.-M. (1999), "Monte Carlo Estimation of Bayesian Credible and HPD Intervals," *Journal of Computational and Graphical Statistics*, 8, 69–92. [1161]

Chiu, S. N., Stoyan, D., Kendall, W. S., and Mecke, J. (2013), *Stochastic Geometry and Its Applications*, Chichester: Wiley. [1155]

Do Carmo, M. P. (2016), *Differential Geometry of Curves and Surfaces: Revised and Updated* (2nd ed.), Mineola, NY: Courier Dover Publications. [1162]

Dryden, I. L., and Mardia, K. V. (2016), *Statistical Shape Analysis: With Applications In R* (Vol. 995), Chichester: Wiley. [1155]

Elliot, P., Wakefield, J. C., Best, N. G., and Briggs, D. J. (2000), *Spatial Epidemiology: Methods and Applications*, Oxford: Oxford University Press. [1155]

Fitzpatrick, M. C., Preisser, E. L., Porter, A., Elkinton, J., Waller, L. A., Carlin, B. P., and Ellison, A. M. (2010), "Ecological Boundary Detection Using Bayesian Areal Wombling," *Ecology*, 91, 3448–3455. [1155]

Gallier, J., and Gallier, J. H. (2000), *Curves and Surfaces in Geometric Modeling: Theory and Algorithms*, San Francisco, CA: Morgan Kaufmann. [1161]

Gao, L., Banerjee, S., and Ritz, B. (2022), "Spatial Difference Boundary Detection for Multiple Outcomes Using Bayesian Disease Mapping," *Biostatistics*, kxac013. DOI:10.1093/biostatistics/kxac013 [1155]

Gleyze, J. F., Bacro, J. N., and Allard, D. (2001), "Detecting Regions of Abrupt Change: Wombling Procedure and Statistical Significance," in *geoENV III — Geostatistics for Environmental Applications*, eds. P. Monestiez, D. Allard and R. Froidevaux, pp. 311–322, Dordrecht: Springer. [1155]

Greenwood, J., (1984), "A Unified Theory of Surface Roughness," *Proceedings of the Royal Society of London*, Series A, 393, 133–157. [1155]

Haining, R. (1993), *Spatial Data Analysis in the Social and Environmental Sciences*, Cambridge: Cambridge University Press. [1155]

Harrison Jr, D., and Rubinfeld, D. L. (1978), "Hedonic Housing Prices and the Demand for Clean Air," *Journal of Environmental Economics and Management*, 5, 81–102. [1162]

Heaton, M. J. (2014), "Wombling Analysis of Childhood Tumor Rates in Florida," *Statistics and Public Policy*, 1, 60–67. [1155]

Heaton, M. J., Datta, A., Finley, A. O., Furrer, R., Guinness, J., Guhaniyogi, R., Gerber, F., Gramacy, R. B., Hammerling, D., Katzfuss, M. et al. (2019), "A Case Study Competition Among Methods for Analyzing Large Spatial Data," *Journal of Agricultural, Biological and Environmental Statistics*, 24, 398–425. [1166]

Hu, L., He, S., Han, Z., Xiao, H., Su, S., Weng, M., and Cai, Z. (2019), "Monitoring Housing Rental Prices Based on Social Media: An Integrated Approach of Machine-Learning Algorithms and Hedonic Modeling to Inform Equitable Housing Policies," *Land Use Policy*, 82, 657–673. [1162]

Jones, C. B. (2014), *Geographical Information Systems and Computer Cartography*, London: Routledge. [1155]

Kent, J. T. (1989), "Continuity Properties for Random Fields," *The Annals of Probability*, 17, 1432–1440. [1155]

Kent, J. T., Mardia, K. V., and Taylor, C. C. (2008), "Modelling Strategies for Bivariate Circular Data," in *Proceedings of the Leeds Annual Statistical Research Conference, The Art and Science of Statistical Bioinformatics*, pp. 70–73, Leeds: Leeds University Press. [1166]

Law, A. M., Kelton, W. D., and Kelton, W. D. (2000), *Simulation Modeling and Analysis* (Vol. 3), New York: McGraw-Hill. [1155]

Lawson, A. B. (2013), *Statistical Methods in Spatial Epidemiology*, Chichester: Wiley. [1155]

Leenaers, H., Schouten, C., and Rang, M. (1988), "Variability of the Metal Content of Flood Deposits," *Environmental Geology and Water Sciences*, 11, 95–106. [1165]

LeSage, J., and Pace, R. K. (2009), *Introduction to Spatial Econometrics*, Boca Raton, FL: Chapman and Hall/CRC. [1155]

Li, P., Banerjee, S., Hanson, T. A., and McBean, A. M. (2015), "Bayesian Models for Detecting Difference Boundaries in Areal Data," *Statistica Sinica*, 25, 385–402. [1155]

Liang, S., Banerjee, S., and Carlin, B. P. (2009), "Bayesian Wombling for Spatial Point Processes," *Biometrics*, 65, 1243–1253. [1155]

Lu, H., and Carlin, B. P. (2005), "Bayesian Areal Wombling for Geographical Boundary Analysis," *Geographical Analysis*, 37, 265–285. [1155]

Magnus, J. R., and Neudecker, H. (1980), "The Elimination Matrix: Some Lemmas and Applications," *SIAM Journal on Algebraic Discrete Methods*, 1, 422–449. [1156]

Majumdar, A., Munneke, H. J., Gelfand, A. E., Banerjee, S., and Sirmans, C. (2006), "Gradients in Spatial Response Surfaces With Application to Urban Land Values," *Journal of Business & Economic Statistics*, 24, 77–90. [1155]

Mardia, K., Kent, J., Goodall, C., and Little, J. (1996), "Kriging and Splines with Derivative Information," *Biometrika*, 83, 207–221. [1157]

Matérn, B., (2013), *Spatial Variation* (Vol. 36), New York: Springer. [1156]

Morris, M. D., Mitchell, T. J., and Ylvisaker, D. (1993), "Bayesian Design and Analysis of Computer Experiments: Use of Derivatives in Surface Prediction," *Technometrics*, 35, 243–255. [1155]

Pebesma, E., Bivand, R., Pebesma, M. E., RColorBrewer, S., and Collate, A. (2012), "Package 'sp,'" *The Comprehensive R Archive Network*. [1163]

Plant, R. E. (2018), *Spatial Data Analysis in Ecology and Agriculture Using R*, Boca Raton, FL: CRC Press. [1155]

Plummer, M., Best, N., Cowles, K., and Vines, K. (2015), "Package 'coda,'" Available at *http://cran.r-project.org/web/packages/coda/coda.pdf*, accessed January 25, 2015. [1161]

Qu, K., Bradley, J. R., and Niu, X. (2021), "Boundary Detection Using a Bayesian Hierarchical Model for Multiscale Spatial Data," *Technometrics*, 63, 64–76. [1155]

Quick, H., Banerjee, S., and Carlin, B. P. (2015), "Bayesian Modeling and Analysis for Gradients in Spatiotemporal Processes," *Biometrics*, 71, 575–584. [1166]

Rudin, W. (1976), *Principles of Mathematical Analysis* (Vol. 3), New York: McGraw-Hill. [1158]

Santner, T. J., Williams, B. J., Notz, W. I., and Williams, B. J. (2003), *The Design and Analysis of Computer Experiments* (Vol. 1), New York: Springer. [1155]

Schabenberger, O., and Gotway, C. A. (2017), *Statistical Methods for Spatial Data Analysis*, Boca Raton, FL: CRC Press. [1155]

Schnare, A. B., and Struyk, R. J. (1976), "Segmentation in Urban Housing Markets," *Journal of Urban Economics*, 3, 146–166. [1163]

Spivak, M. (1999), *A Comprehensive Introduction to Differential Geometry*, in *A Comprehensive Introduction to Differential Geometry* (Vols. 1–5), Houston, TX: Publish or Perish Inc. [1162]

Stein, M. L. (1999), *Interpolation of Spatial Data: Some Theory for Kriging*, New York: Springer. [1155,1156,1157]

Stevens, K. A. (1981), "The Visual Interpretation of Surface Contours," *Artificial Intelligence*, 17, 47–73. [1156]

Terres, M. A., and Gelfand, A. E. (2015), "Using Spatial Gradient Analysis to Clarify Species Distributions With Application to South African Protea," *Journal of Geographical Systems*, 17, 227–247. [1155]

Terres, M. A., and Gelfand, A. E. (2016), "Spatial Process Gradients and their Use in Sensitivity Analysis for Environmental Processes," *Journal of Statistical Planning and Inference*, 168, 106–119. [1155]

Vaughan, L. (2018), *Mapping Society: The Spatial Dimensions of Social Cartography*, London: UCL Press. [1155]

Waller, L. A., and Gotway, C. A. (2004), *Applied Spatial Statistics for Public Health Data* (Vol. 368), Hoboken, NJ: Wiley. [1155]

Wang, F., Bhattacharya, A., and Gelfand, A. E. (2018), "Process Modeling for Slope and Aspect with Application to Elevation Data Maps," *Test*, 27, 749–772. [1155,1157,1166]

Wang, X., and Berger, J. O. (2016), "Estimating Shape Constrained Functions Using Gaussian Processes," *SIAM/ASA Journal on Uncertainty Quantification*, 4, 1–25. [1155]

Webster, R., and Oliver, M. A. (2007), *Geostatistics for Environmental Scientists*, Chichester: Wiley. [1155]

Williams, C. K., and Rasmussen, C. E. (2006), *Gaussian Processes for Machine Learning* (Vol. 2), Cambridge, MA: MIT Press. [1157]

Winkler, G. (2003), *Image Analysis, Random Fields and Markov Chain Monte Carlo Methods: A Mathematical Introduction* (Vol. 27), Berlin: Springer. [1155]

Wise, S., and Craglia, M. (2007), *GIS and Evidence-Based Policy Making*, Boca Raton, FL: CRC Press. [1155]

Womble, W. H. (1951), "Differential Systematics," *Science*, 114, 315–322. [1155]